Comparison of Thermal Annealing versus Hydrothermal Treatment Effects on the Detection Performances of ZnO Nanowires

Oleg Lupan, Nicolae Magariu, Rasoul Khaledialidusti, Abhishek Kumar K Mishra, Helge Krüger, Sandra Hansen, Vasile Postica, Helge Heinrich, Bruno Viana, Luis Katsuya K Ono, et al.

Comparison of Thermal Annealing vs Hydrothermal Treatment Effects on the Detection Performances of ZnO Nanowires

O. Lupan,[*,1,2,3,4] N. Magariu,[3] R. Khaledialidusti,[*,5] A.K. Mishra,[*,6] H. Krüger,[2] S. Hansen,[*,2] V. Postica,[3] H. Heinrich,[4,7] B. Viana,[1] L.K. Ono,[4,8] B. Roldan Cuenya,[4,9] L. Chow,[4] R. Adelung,[*,2] Th. Pauporté[1]

[1] *Institut de Recherche de Chimie Paris-IRCP, Chimie ParisTech, PSL Université, 11 rue Pierre et Marie Curie 11, 75005 Paris, France*

[2] *Functional Nano Materials, Institute for Materials Science, Faculty of Engineering, Kiel University, str. Kaiserstraße 2, D-24143 Kiel, Germany*

[3] *Center for Nanotechnology and Nanosensors, Department of Microelectronics & Biomedical Engineering, Technical University of Moldova, Stefan Cel Mare Av. 168, MD 2004 Chisinau, Republic of Moldova*

[4] *College of Sciences, Physics Department, UCF Florida, 41111 Libra Drive str., FL32816, USA*

[5] *Department of Mechanical & Industrial Engineering at Norwegian University of Science & Technology, 74911, Trondheim, Norway*

[6] *Physics Department, Engineering School, University of Petroleum & Energy Studies, Bidholi via Premnagar, Dehradun, 248007, India*

[7] *Department of Materials Science & Engineering, University of Virginia, 395 McCormick-Road Charlottesville, VA-229044, USA*

[8] *Energy Materials and Surface Sciences Unit, Okinawa Institute of Science and Technology Graduate University, Okinawa 9044-0495, Japan*

[9] *Department of Interface Science, University of Fritz Haber Institute of the Max Planck Society, Berlin, Germany*

Phone: +49 431 880 6335, Fax: ++49 431 880 6124/6229,

e-mails: ollu@tf.uni-kiel.de oleg.lupan@mib.utm.md

* Corresponding authors:

Prof. Dr. O. Lupan (ollu@tf.uni-kiel.de)
Institute of Materials Science, University of Kiel, Kaiserstr. 2, D-24143, Kiel, Germany

Prof. Dr. R. Adelung (ra@tf.uni-kiel.de)
Kiel University, Germany

Prof. Dr. A.K. Mishra (akmishra@ddn.upes.ac.in)
University of Petroleum & Energy Studies, India

Dr. Rasoul Khaledialidusti (rasoul.khaledialidusti@ntnu.no)
NTNU, Norway

Keywords: ZnO, Nanowires, Electrodeposition, Photoluminescence, Nanosensors.

ABSTRACT

A comparative investigation of the post-electroplating treatment influence on the gas detecting performances of single ZnO nanorod/nanowire (NR/NW), grown by electrochemical deposition (ECD) and integrated into nanosensor devices is communicated. In this work, hydrothermal treatment-(HT) in water (H_2O) vapors and conventional thermal annealing-(CTA) in a furnace at 150 °C in air were used as post-growth treatments to improve the material properties. Herein, the morphological, optical, chemical, structural, vibrational, and gas sensing properties of the electrodeposited and treated samples are investigated and presented in detail. By varying the growth temperature and type of post-growth treatment, the morphology is maintained, whereas the optical and structural properties show increased sample crystallization. It is shown that HT in H_2O vapors affects the optical properties of the material. After investigation of nanodevices based on single ZnO NR/NWs, it was observed that higher temperature during synthesis possess results in a higher gas response to H_2 gas within the investigated operating temperature range from 25 °C to 150 °C. Density functional theory (DFT) calculations for ZnO surfaces provide insights into structure and electronic bands changes because of H_2 gas molecules, indicating strong interaction between the surface and the H_2 molecules. CTA and HT or autoclave treatment (AUT) showed the capability of a further increase in gas response of the prepared sensors by a factor of ~8. Our results demonstrate that high-performance devices can be obtained with high-crystallinity NWs/NRs after HT. The obtained devices could be key element for flexible nanoelectronics, wearable electronics and have attracted a great interest due to its unique specifications.

1. INTRODUCTION

Quasi-one-dimensional (Q-1D) micro- and nano-structures, like wires, rods, fibers and tubes of metal oxides are key elements for nanoelectronics, especially flexible one, wearable electronics, including nanosensors, and have attracted a great interest in research of high-performance devices with unique specifications. [1-3] ZnO Q-1D nanostructures are considered due to their essential application potential, [2,4] e.g. optoelectronic microdevices or even flexible nanoelectronics, [4-6] gas nanosensors, [3,7,8] light emitting diodes, [9,10] transistors, etc. [11]

Different techniques have been engaged to fabricate ZnO NWs/NRs, including chemical and physical methods,[10,12-15] as well as different methods were used to enhance the gas sensing properties. For example, Drobek *et al.* report on a general methodology for improving the selectivity of semiconductor metal oxides nanowires sensors, based on the coverage of ZnO nanowires with a thin molecular sieve membranes.[16-19] Among the wide range of techniques, ECD has become an advantageous technique for synthesis of ZnO Q-1D structures, being cost-efficient and having a possibility of large-area deposition of structures with excellent optical properties. Furthermore, NWs/NRs can be deposited at lower temperatures in comparison with other techniques.[12,20,21] ECD method also allows the efficient doping of ZnO NWs/NRs with a diversity of ion metals, namely Cd, Eu, Ag, Cu, Cl, Al, etc.[5,22-26] Recently, the one-step surface doping and functionalization with Pd and Au nanoparticles was achieved by ECD method.[8,24,27,28] Based on individual nano- and microstructures grown by ECD method, such as Ag-doped ZnO NW, Au-modified NW, Pd-modified ZnO NW, high performance nanosensors for the detection of H_2 gas in the operating temperature range 25 – 150 °C were shown.[5,24,29] For example, by Al-doping of ZnO NWs it is possible to detect volatile organic compounds at room temperature with excellent long-term stability.[22] Another advantage of ECD method is the synthesis of ZnO NWs on flexible

substrates,[30] this point being important for application in flexible and wearable electronics, including gas sensors and UV photodetectors.[31,32]

While the doping and surface functionalization effect on ultraviolet light and gas detecting performances of single ZnO NRs/NWs, obtained by ECD method, have been studied extensively, less attention was paid on the influence of post-deposition thermal treatment. Previous works revealed that thermal treatment of ZnO NWs has an essential influence on structural and optical properties of samples.[33,34] But, conventional thermal annealing (CTA) could not be realized on flexible or other substrates for wearable electronics, which do not survive to high temperatures due to melting or deterioration processes.

Thus, a thorough comparison of the influence of post-synthesis temperature treatments, like hydrothermal treatment (HT), autoclave treatment (AUT) or CTA in different ambient (air or in water vapor ambient) is essential, especially the effect on the gas sensing properties of electrodeposited ZnO NWs/NRs grown from a chloride medium.[30,33] The post-growth thermal annealing in air and hydrothermal treatment in water vapor ambient are important methods for improving the quality of the ECD ZnO NWs/NRs and changing its surface properties.[10,33] Because the sensing properties of individual nanostructures with high surface-to-volume ratio are highly dependent on surface properties,[5] the stabilizing effect for future devices on flexible substrates is expected.

The ZnO NR/NW arrays studied here were grown by ECD followed by post-growth HT in H_2O vapor and CTA in normal ambient at the same temperatures and durations for comparison studies.[34] The structural, chemical, vibrational, optical, and sensor performances of the as-electroplated and treated samples were investigated in detail. The individual ZnO NRs/NWs were incorporated into micro-devices employing focused ion beam/scanning electron microscopy (FIB/SEM) equipment. The gas and UV detection measurements demonstrate that the performances of the fabricated devices can be significantly improved by

increasing the electrodeposition temperature, as well as by the post-growth treatment, especially by HT with water vapors at 150 °C for 12 h. The results obtained in this research work represent a meaningful step headed for the elaboration of higher-performance gas sensor devices based on a single ZnO NR/NW.

2. EXPERIMENTAL DETAILS

2.1. Electroplating

ZnO NR/NW arrays were grown by the electrodeposition approach from a 0.20 mM $ZnCl_2$ (99.5%) solution in H_2O hold at 70°C, then increased with a step of 10 °C/specimen up to 90°C, as reported elsewhere.[10,30,33,34] 0.1 M of KCl (Fluka, 98%) was accessed as an additive, to confirm a reliable electrical conductivity in the H_2O – based electrolyte.[33] Based on reports on the synthesis of ZnO by electrodeposition, the chloride content is always higher (> ~22 times) than the zinc content in the ECD solution.[14,20,21,33] The ZnO NRs/NWs were electrodeposited on a glass substrate having a conductive fluorine-tin-oxide (FTO) layer on top (sheet resistance of 10 Ω/□).[5,10,24,29] The FTO/glass was employed as the working electrode (WE) in a classical 3 electrode setup for electrodeposition of ZnO NRs/NWs.[14,20,21,33] Before ECD, the FTO substrates were cleaned in an ultrasonic bath first with acetone, then C_2H_5OH (100%) for 5 min each and rinsed afterwards with deionized H_2O (18.22 MΩ·cm) for 10 s.[14,20,21,25,33] The substrates with FTO layer were dipped in HNO_3 (45%) for 60 s and also rinsed with deionized H_2O in the ultrasonic bath for 5 min.[33] The cleaned substrate with FTO layer was attached to a rotating working electrode.[33] The reference electrode was mounted in a separated cell arm-tube at room temperature as reported in previous works.[8,22,33] The counter electrode (CE) used during the electrodeposition was a platinum (Pt) spiral-wire.[33] The ECD process was done at –1.0 V controlled with an Autolab PGSTAT30a galvanostat/potentiostat,[33] monitored by the AutoLab software. The WE was

rotated constantly with a speed ω=300 rot/min.[28,35] The pH-value of the ECD bath in the beginning was around 5.50.[35] The ECD cell was introduced in a larger second bath with thermoregulation and kept constant at 70°C, 80°C or 90°C,[35] with an uncertainty of ± 0.2 °C for three different experiments, respectively.[10] The electrolyte was saturated with extra pure O_2 for 50 min prior and during the ECD.[26,27] The ECD for the syntheses of ZnO NR/NW arrays on FTO was stopped when the passed electrical charge during synthesis was about 15.4 $C \cdot cm^{-2}$ at 70°C, 14.3 $C \cdot cm^{-2}$ at 80°C and 11.2 $C \cdot cm^{-2}$ [26]

The main physicochemical reactions during the cathodic zinc oxide NR/NW array growth in an aqueous $ZnCl_2$ solution can be described as followed:[33,36]

$$O_2 + 2H_2O + 4e^- \rightarrow 4OH^- \qquad E^o = 0.4V / NHE \qquad (1)$$

The oxygen reduction reaction in electrochemical process proceeds:[37,38]

$$Zn^{2+} + 2(OH)^- + 4e^- \rightarrow Zn(OH)_2 \xrightarrow{\Delta} ZnO + H_2O \qquad E^o = 0.4V / NHE \qquad (2)$$

ZnO NRs/NWs are grown as following:[33,36]

$$Zn^{2+} + \frac{1}{2}O_2 + 2e^- \rightarrow ZnO \qquad E^o = 0.93V / NHE \qquad (3)$$

The ZnO NWs/NRs were ECD on FTO at –1.0 V, and the changes with time of electrical current density (j) was saved in AutoLab software.[33] **Figure S1** represents the time dependent changes of electrical current density for electrodeposition of ZnO NWs/NRs at 70 °C, 80 °C and 90°C. The illustrated curves indicate clearly that the ECD ZnO NR/NW are electrical

conductors, due to the electrical current densities collected at the electrode that are maintained at necessary values.[39] Steady state current densities of pure zinc oxide NRs/NWs are about 1.9 (at 70°C), 1.8 (at 70°C) and 1.2 $mA \cdot cm^{-2}$ (at 90°C) after 3000 seconds of ECD. **Figure S2** shows the cyclic voltammograms on FTO substrates for specimens grown at 70 °C and 80 °C measured with a scanning rate of 11 $mV \cdot s^{-1}$.[25] As can be observed the cathodic wave starts at about − 850 mV vs saturated calomel electrode (SCE). The maximum current density was about 1.13 mA/cm^2 at − 1.29 V vs SCE for specimens grown at 70°C and 1.26 mA/cm^2 at − 1.29 V vs SCE at 80°C. This peak can be designated to the electrochemical reduction of molecular oxygen.[25,26] The small hysteresis, observed in both cases can be described by large coverage on the FTO surface/substrate with zinc oxide NRs/NWs upon the forward scan.[25,26]

After the ECD process, the prepared ZnO NRs/NWs were first dipped with DI-H_2O to clean the sample from chloride salts and other unwanted species and then cut into three equal parts.[10] Whereas one part was used as the reference specimen, the other two parts were heat treated using CTA and HT at 150°C in air for 12 h and post-growth hydrothermal treatment at 150°C for 12 h in water vapor ambient, respectively.[33,34] The hydrothermal treatment ~~(AUT)~~ was performed at 150°C in a stainless steel autoclave with an inner liner of 100 mL made from Teflon.[10,30] To exclude the direct contact of ZnO NWs/NRs with water, the sample was fixed at 3.5 cm above the DI H_2O surface.[10,30] Thus, to evaluate the influence of CTA and HT on the ZnO NWs/NRs three sample sets were prepared in the same conditions.

2.2. Characterization of electrochemically prepared ZnO NWs/NRs and fabrication of gas nanosensors

Details of the experimental procedures, as well as samples characterization methods can be found in previous reports.[10,25,33,40,41] To investigate the effect of HT and CTA on the gas sensing performances of samples, the prepared nano- and microstructures were integrated

into nanodevices. The procedure of nanodevice fabrication using ~~focused-ion-beam/scanning-electron-microscope (FIB/SEM)~~ FIB/SEM equipment can be found elsewhere (see references).[4,5,7] According to this technique up to eight individual nano- and microstructures of different oxides and other materials with diameter down to 20-30 nm can be integrated in one device [42] consisting of a specially designed chip based on a SiO_x/Si 800 nm substrate with pre-patterned Au/Cr contacts.[28] The individual structures were contacted with Au pre-pads using the electron beam maskless Pt complex nanodeposition in a dual beams FIB/SEM instrument to avoid Ga implantation or Ga milling when using Ga for Pt complex deposition. The Dual beams (FEI) (5.0 kV, 0.175 nA),[5] forming the Au/Pt/ZnO/Pt/Au structures with two contacts. The electrical and gas detection measurements were realized as reported elsewhere.[5,7,43]

2.3. Computational Details

Computational studies are performed using the DFT and its generalized gradient approximation (GGA). The Perdue–Burke–Ernzerhof (PBE)[44] exchange–correlation functional and the projected augmented wave (PAW)[45,46] approach was used through its implementation in the Vienna *ab initio* Simulation Package (VASP).[47] Using the conjugate gradient method,[48] the bulk structure of ZnO was fully optimized till the maximum residual force acting on each atom becomes < 0.00010 eV/Å. The energy convergence criterion used is $1 \cdot 10^{-7}$ eV/cell having a plane wave cutoff energy of 520 eV. For modelling the bulk ZnO structure, 5 × 5 × 4 Monkhorst-Pack *k* points were used,[49] while surfaces are computed using the 4 × 4 × 1 Monkhorst-Pack *k* points. For the determination of the Methfessel–Paxton smearing scheme partial occupancies with smearing width of 0.10 eV were used. A vacuum space of 20.0 Å was used to avoid any interaction with a ZnO (0001)/ZnO $(10\bar{1}0)$ surface and its periodically repeated images along the *c* axis. Surface energies were calculated using a

combination of calculations for the relaxed and unrelaxed surfaces[74]. Here, the Coulomb effect (U) for the localized 3d electrons of metal atoms were investigated and a negligible effect on the results was obtained, hence this is not incorporated in the calculations.

The DFT- D2 approach as described by Grimme[50] was used to incorporate the long-range dispersion corrections while investigating gas molecule interactions. The adsorption energy of a gas molecule was computed using the:

$$E_{ads} = E_{surf+mol} - (E_{surf} + E_{mol}) \quad (4)$$

where $E_{complex}$ - total energy of the surface with molecule, $E_{surface}$ - energy of the surface slab without molecule, and $E_{molecule}$ - energy of the isolated molecule. $E_{molecule}$, was calculated by modelling the isolated molecule in the center of a broken symmetry cell with lattice constants of 20 Å, inspecting only the Gamma-point of the Brillouin zone with the same truthfulness specification as construe for the surfaces.

3. RESULTS AND DISCUSSION

3.1. Characterization of structure and morphology characteristics of ZnO NRs/ NWs

Figure 1a illustrates the XRD diffractograms of as-electrodeposited ZnO samples at 70, 80 and 90 °C, while **Figure 1b** exhibits the XRD diffractograms of ZnO samples electrodeposited at 70 °C and treated by AUT and CTA at 150 °C. The peaks which originate from the SnO_2 substrate (according to the PDF 01-077-0488 card [33]) were marked with red dots. The detected reflection with highest intensity is at 2θ values of 34.43°, which correspond to the lattice (002) plane. Other reflections with significantly lower intensity were detected at 31.8°, 36.2°, 47.5°, 56.7°, and 62.8° corresponding to the (100), (101), (102), (110) and (103) lattice planes, respectively. The obtained results show that ZnO NWs/NRs

grow with a (002)-preferred direction, i.e. nanowire arrays have the excellent overall *c*-axis alignment arrays over the large FTO substrate area.

From **Figure 1b** it can be observed that after AUT and CTA treatment at 150 °C the intensity of the peak corresponding to the (002)-plane remains with higher intensity in comparison to other peaks, demonstrating that post-growth thermal treatment ~~do~~ does not induce changes in orientation of ZnO NWs/NRs in the *c*-axis. The full width at half-maximum (FWHM) values of the (002) peak of oxide NWs/NRs arrays on FTO substrate are 0.1248°, 0.0936° and 0.0930° (see **Figure 1b**) for the samples as-deposited, after CTA and AUT at 150°C, respectively. These low values of FWHM widths indicate a high crystallinity of the electrodeposited material, even at lower temperature of 70 °C, which can be further improved by AUT or CTA treatment.[33]

SEM investigations were selected to characterize the morphology of the as-electrodeposited NWs/NRs and the influence of AUT and CTA treatment (see **Figure 2**). The aspect ratio of ZnO NWs/NRs were not changed essentially after annealing, following recent results on ZnO samples synthesized by ECD method.[33,39] According to the top view and the cross-section (see **Figure 2**) a diameter of 70-100 nm was estimated. For samples electrodeposited at 70 °C the average diameter (*D*) of ~ 100 nm is the same for the entire surface having high uniformity and a fully covered surface. The length of NRs is ~ 1 μm with a clearly observable hexagonal end planes. No significant changes in morphology after CTA or AUT treatments at 150 °C were observed. However, after AUT ~~a~~ smoother surfaces of the NRs can be observed. For samples grown at 80 °C, the NRs are thinner in diameter than those grown at 70 °C, with a diameter of D ~ 70 - 90 nm, and a length of ~ 2 μm. Also for these samples, the average NR-diameter are almost similar across the entire surface. It can be observed that nanowires are quasi-aligned (see **Figure 2**). For samples grown at 90°C, the ZnO NWs/NRs with a wider range of diameters is found. The individual diameters of the

structures are non-uniform, varying between 70 - 200 nm, while the average length is about ~ 3 μm. In **Figure 2** the influence of the growth rate is observable showing an increasing rate for samples electrodeposited at 70°C to 80°C and 90°C; even though the electrical current density is highest for samples deposited at 70°C. As can be seen, the treatment does not cause any significant changes, which is in accordance with the above reported XRD results. However, after being post-growth AUT-treatment at 150°C for 12 h in water vapors, the lateral facets become smoother (see **Figure 2f**).

Transmission electron microscopy (TEM) was operated to find the properties of structure for the as-electrodeposited zinc oxide NRs/NWs, in conjunction with study the influence of AUT and CTA treatment. **Figure 3** reports typical TEM and high-resolution TEM (HRTEM) images presenting the general morphology of the electrodeposited ZnO NRs-nanorods grown at 70, 80 and 90°C. Nanorods grown at 70°C (see **Figure 3a**) are about 100nm in diameter and 1.3 μm in length. It is also important to note that the diameter varies along the nanorod length (see **Figure 3a**). This phenomenon is less manifested for the nanorods grown at 80 °C. According to our observations, the TEM images (see **Figure 3b**) show that the diameter is uniform from one nanorod to another for the same sample electrodeposited at 80 °C. The tip of the NR is round-shaped with about 10 nm radius, as presented in **Figures 3a, 3b**. In the case of samples electrodeposited at 90 °C (see **Figure 3c**) a higher diameter of 100 – 200 nm was observed. The atomic arrangements of the ZnO nanorods are seen in **Figure 3d-f**, showing that ZnO NWs/NRs grow along the [0001] direction, which is in concordance with XRD data.[51] The calculated distance between ZnO (0001) fringes perpendicular is 0.26 nm.[51] Also, it confirms that the NR has a single crystalline structure in the investigated area. The obtained results confirm that the zinc oxide NRs/NWs are well-crystalline possessing a hexagonal crystal lattice.

Typical selected area electron diffraction (SAED) patterns of ZnO NRs/NWs electrodeposited at 70°C, 80°C and 90°C are presented in **Figure 3g-i**. Independent of the electrodeposition temperature the ZnO NRs/NWs are single crystalline with distinct diffraction spots, and, to a smaller extent, nanocrystalline with diffuse diffraction rings.[52,53]

3.2. Chemical characterizations (EDX and XPS)

For a characterization of the chemical composition of ZnO NRs/NWs, energy dispersive x-ray spectroscopy (EDX) analysis at the TEM was performed. **Figure S3** represents the EDX spectrum of individual ZnO NW scratched from the electrodeposited material on the FTO substrate. Here, peaks of the two essential constituent's Zn and O in the zinc oxide nanorod/nanowire can be distinguished, as well as peaks of C and Cu originating from the holey carbon film and the copper TEM grid. No evidence of other impurities was found in the EDX spectrum.

X-ray photoelectron spectroscopy (XPS) were performed to investigate the chemical characteristics of electrodeposited ZnO nanomaterial in chloride medium in more detail, as well as the effect of AUT and CTA post-growth treatment. The adventitious carbon peak (C-1s) at 285.0 eV was used as a reference in order to calibrate the binding energy.[33,54,55] Because all samples were maintained in air before measurements, the presence of residual quantities of adventitious carbon/carbonyl conglomerate are inevitable.[33,56]

XPS survey spectra are demonstrated in **Figure S4**, from which the following elements were detected: O, Zn, C (adventitious), and Sn. The Sn signal originates from the FTO substrate. The low intensity peaks detected at ~ 230 eV and ~ 400 eV for as-grown sample at 70 °C can be attributed to Mo-3p and Mo-3d core levels, respectively, which can originate from the partially exposed sample holder.[34] No other elements or else from the electrodeposition bath were detected. **Figure 4** presents XPS spectra of the core level regions

for (a) Zn-2p and (b) O-1s of the synthesized samples. The ZnO NRs/NWs display a doublet at 1021.71 eV and 1044.81 eV and can be associated to the core levels Zn-$2p_{3/2}$ and Zn-$2p_{1/2}$ from ZnO (see **Figure 4a**).[33] These binding energy (BE) values are in agreement with previously prepared pure ZnO samples from our group.[20,54,57] The presence of residual Cl compounds from our preparation method was discarded based on XPS measurements from the Cl-2p BE region (not shown), in agreement with previous works.[33,58] No detectable amounts of Cl were observed in our XPS measurements, which are in accordance with EDX studies performed from a single ZnO NW in TEM. The asymmetric peak detected in the region of O-1s, **Figure 4b**, was deconvoluted by sub-spectral components: stoichiometric ZnO (530.21 eV) (i), defective ZnO_x (531.61 eV) (ii), adventitious CO (531.11 eV) (iii),[59] and adventitious CO_2 (532.51 eV) (iv).[60-62] The relative content of each compound is shown in **Table 1**. The $ZnO_x(OH)_y$ stoichiometry was considered using the intensity ratios of O-1s/Zn-2p peaks.[33,63]

The peak observed in the O-1s region is asymmetric (see **Figure 4b)** and thus deconvoluted by 4 components: (i) stoichiometric ZnO (530.20 eV), (ii) defective ZnO_x (531.60 eV), (iii) adventitious CO (531.10 eV),[59] and (iv) adventitious CO_2 (532.50 eV).[60,61] **Table 1** illustrate the relative content of each compound extracted from the fittings. Zordan *et al.*[63] and Jiazhong *et al.*[64] detected similar components in their O-1s spectra and assigned the high BE peak (531.60 eV) to Zn-OH species. Because of their O-1s/Zn-2p ratios, the stoichiometry of $ZnO_x(OH)_y$ have been proposed.[63] The 531.60 eV component found in investigated specimens may assign to $ZnO_x(OH)_y$. Furthermore, it is reported that ZnO_x defective is reduced after HT.[63] The XPS spectra of CTA samples was presented in the previous work and shows the similar effect and spectral features.[33]

3.3. Micro Raman scattering

Figure 5 illustrates the micro Raman spectra of the ZnO NRs/NWs electroplated on FTO recorded at room temperature. For all samples, the presence of high intensity vibrations at 440 and 100.1 cm^{-1} is characteristic, corresponding to E_{2high} and E_{2low} modes, accordingly. The broad peaks marked with red dots can be attributed to FTO substrate.[33] The presence of weak peak at 410.1 cm^{-1} corresponds to E_{1TO} mode.[65] Because the Raman selection rules predict that TO modes are forbidden in the case of incident light parallel to the *c* axis of ZnO NWs/NRs, the presence of E_{1TO} mode can suggest that not all structures are perpendicularly to the substrate.[66] Therefore, it could be suggested that ZnO NWs/NRs are quasi-*c*-axis oriented, which is in conformity with previous SEM results.[66] From **Figure 5a** the increase in intensity of modes E_{2high} and E_{2low}, characteristic of the wurtzite lattice, caused by the increase in synthesis temperature from 70 to 90 °C can be observed. **Figures 5b-d** show that the AUT and CTA treatments results in further increase in intensity and sharpening of E_{2high} and E_{2low} modes. Moreover, the AUT treatment results in better samples crystallization i.e. is more effective in improving the optical properties.[30,34,67] From **Figure 5** it can be observed that intensity of E_{2high} and E_{2low} modes is increasing after AUT or CTA treatment in all investigated cases, independent on the growth temperature, which also can indicate on increased crystal quality of the treated samples.[30,34,67]

3.4. Optical characterization

Transmission spectra of ZnO NWs electrodeposited on a substrate covered with FTO at 60 °C, 70 °C, 80 °C and 90 °C are presented in **Figure 6**. For all samples the excellent transparency in the visible range and in the UV region (over 90%) was observed. It was found that the optical transmittance can be enhanced by a rise in temperature of the ECD bath, which can be associated to the ~~raise in the crystallinity and a~~ decrease in surface roughness, as

observed during SEM and TEM studies (see above). No essential shift in absorption edge was observed.

Figure 7 illustrates the photoluminescence spectroscopy (PL) spectra of ZnO NRs/NWs, recorded at room temperature. The PL spectra demonstrate a high UV and a low visible emission peak in the as-deposited ZnO nanostructures. The UV line for the as-electrodeposited ZnO at about 381 nm is assigned to a free exciton and a neutral donor bound exciton.[33] No shift UV exciton-related emission peak was observed for heat treated samples, i.e. by AUT or CTA.[33]

The FWHM values of the UV peaks from all samples are ranging from 1400 to 2000 cm^{-1}. This could be explained as after annealing, the variation of defects can take place as follows:[68,69]

$$V_O + \frac{1}{2}O_2 = O_O \tag{5}$$

$$Zn_i + \frac{1}{2}O_2 = Zn_{Zn} + O_O \tag{6}$$

where $[Zn_i]$, $[Zn_{Zn}]$ and $[O_O]$ are the concentrations of the interstitial Zn, Zn in the lattice place and oxygen in the lattice place, respectively. These equations show that by an increase in treatment temperature during ECD of ZnO NWs/NRs, a decrease in defect concentration can be obtained.[33] Therefore, it was observed that the intensity of the UV peak increases and the intensity of the visible PL emission peak decreases.[33] For thermal treated ZnO NWs/NRs, the visible PL emission peak is difficult to see from the inset of **Figure 7**. The ratio between intensity of the near-band-edge (NBE) UV vs the visible PL emissions is about 42 for the as-grown sample and 50 and even 100 for the AUT annealed samples, respectively.

From **Figure 7a** it could be observed that samples electrodeposited at 80 °C have a higher emission at the band-gap emission compared to samples electrodeposited at 70 °C. ZnO NWs electrodeposited at 90 °C has the highest near-bandgap emission. The visible emission was not observed as the intensity is two orders of magnitude lower than the UV emission. According to the data reported in **Figure 7b-d** it can be concluded that synthesized samples that were subjected to CTA at 150 °C for 12 h in air, independent of the growth temperature, show an increase in UV emission. However, samples after AUT treatment in ambient H_2O vapors have a higher UV emission compared to CEA samples or as grown samples. These experimental data are ~~is~~ in concordance with ~~T-A,~~ XRD, Raman and XPS data. Thus, the increased UV emission intensity after CTA or HT can be a result of the enhanced crystallinity of the electrodeposited ZnO NWs/NRs as well as a reduced defect concentration in the crystalline material.

3.5. Gas sensing performances of ECD ZnO NRs/NWs

To investigate the room temperature sensing properties of ZnO NRs/NWs electrodeposited at different temperatures, the individual nanostructures were integrated into devices. SEM images of individual as-electrodeposited ZnO NWs/NRs synthesized at 70 °C, 80 °C and 90 °C and integrated on a specially designed chip are presented in **Figure 8a-c**.[28] Because the gas response is highly reliant on the width changes of the surface electron depletion region of ZnO NW/NR due to adsorption/desorption processes of gaseous/vapor species,[70] the use of nanostructures with smaller diameter is crucial for fabrication of high performance gas nanosensors.[70] In our case the ZnO NWs/NRs with a diameter in the same range were integrated. This is of major importance, since the structure diameter value is one of the most significant factors that determine the gas detection properties of devices, especially in the case of individual structures, while the length of NW has a minor role.[28,42]

Also, the dependence of the gas sensitivity on various temperatures of the electrolyte growth solution need to be considered. As can be observed from **Figure 8a-c** the diameter of NWs/NRs changes is in the order of 170 to 220 nm along the structure.

The typical current-voltage characteristics of device based on individual ZnO NW grown at 90 °C is presented in **Figure S5a**. Such quasi-linear behavior was observed for all tested samples. This indicates on the formation of low barrier at Pt/ZnO interface and indicates that gas response originates mainly from modulation of electron depletion region, which will be discussed later in gas sensing mechanism. [5,71,72]

The gas sensing performances were investigated in a working temperature ~~vary~~ varying between 25°C – 150°C. Higher operating temperatures were not applied to prevent damage of the Pt/ZnO contacts. **Figure 8d** presents the gas response versus working temperature of devices to 100 ppm of hydrogen gas. According to the obtained data, the gas response is increasing when rising the operating temperature from 25°C to 150°C. Also, a rise in temperature of the electrolyte solution for growth of ZnO NWs/NRs from 70°C to 90°C show a higher gas response. The highest gas response of ~ 60 was obtained for ZnO NW grown at 90°C and measured at a working temperature of 150°C.

In **Figure 9**, the dynamic gas response at 150°C of individual ZnO NW synthesized at 70 °C to multiple exposures of H_2 gas with 100 ppm is presented. Here, the good ~~good~~ repeatability of the fabricated sensors is demonstrated. The residual standard deviation of the gas response for all samples is limited to 10%. In **Figures 9a** and **9b** the dynamic response to H_2 gas with different concentrations at an operating temperature of 150°C for individual ZnO NW synthesized at 80°C and 90°C is presented. A complete recovery of the signal to the starting electrical baseline after evacuating the H_2 gas from the testing chamber is observed. This is very important for real-time application in monitoring of hydrogen gas concentrations. The response time and recovery times for detecting 100 ppm H_2 gas is 26 s and 35 s for NWs grown at 70 °C, 21 s and 20 s for NW grown at 80°C, 17 s and 16 s for NWs grown at 90°C.

Therefore, **Figures 9a-c** indicate that NWs grown at higher temperatures have a faster saturation of the gas response and a faster recovery of the signal.

Figure 9d shows the gas response value versus hydrogen gas concentration at 150 °C for individual ZnO NW/NR synthesized at 70°C, 80°C and 90°C, demonstrating a power law dependence of gas response on hydrogen concentration.[43] The $I_{gas}/I_{air} > 1.2$ criterion was used to determine the lower detection limit (LDL) of the nanosensor.[42] For NWs grown at 70°C, 80°C and 90°C the estimated LDL value is ~ 5 ppm, ~ 1.8 ppm and ~ 1.1 ppm, respectively. Overall, the presented results show that the use of ZnO NWs/NRs grown at the higher temperatures, especially at 90°C, are preferable to fabricate gas nanosensors with higher performances, including gas response, response/recovery time and lowest detection limit.

Next, the influence of post-growth conventional thermal annealing (CTA) in air and hydrothermal (AUT) annealing in water vapors at 150°C for 12 h on the gas detection was investigated. Here, ZnO NWs/NRs grown at 80°C were used. **Figure 10a** presents the response to 100 ppm of H_2 gas as a function of work temperature of individual ZnO NWs and treated with CTA or AUT. As can be observed, the post-growth treatment can lead to a further enhancement of gas response value for the electrochemically deposited ZnO NRs/NWs. The highest increase in response was obtained for AUT by hydrothermal annealing in water vapors. At 150°C, the response value to 100 ppm of H_2 is 45, 93 and 380 for as-grown, CTA and AUT treated ZnO NRs/NWs, respectively. The post-growth annealing does not affect the optimal operating temperature of the specimens showing still the highest response at 150°C.

The time-dependent response at 150°C to 100 ppm of hydrogen gas of single ZnO NW synthesized at 80°C by ECD and treated CTA or AUT is presented in **Figures 10b** and **10c**, respectively, showing excellent repeatability and total recovery of the signal. The responses and recovery times are ~ 5 s and ~ 10 s for CTA treatment and ~ 11 s and ~ 10 s for AUT treatments, respectively. To check the selectivity of the ZnO NRs/NWs, the gas detection

measurements were performed at 150°C working temperature to 100 ppm of ammonia, 2-propanol, butanol, acetone, ethanol and hydrogen (see **Figure 10d**). In all cases, no detectable sensitivity/response to other vapors was found, demonstrating the high selectivity of ZnO NRs/NWs to H_2 gas.

The fabricated nanosensors were also tested under UV light, as reported previously.[68] **Figure S5b** shows the UV response of individual nanowires grown at 70, 80 and 90°C. The UV response value was determined using the relation I_{UV}/I_{Dark}, where I_{UV} and I_{Dark} is the electrical current under UV illumination and in the dark. The UV response of nanowires grown at 70, 80 and 90°C is ~ 3.75, ~ 2.7 and ~ 1.80, respectively. Therefore, the highest UV response was obtained for the nanowire grown at 90°C. Analyzing the given **Figure S5b**, it was noticed that the response times are much shorter than the recovery times. The similar conclusions were reported by Liu *et al.*, i.e. higher UV sensing performances of ZnO NW with higher crystallinity.[73] However, in our study this is demonstrated namely for individual structures, where no influence of NW-NW junction effect is presented.

3.6. Gas sensing mechanism

For single nanostructures of semiconducting oxides the gas sensing mechanism is associated to the surface phenomena.[5,7] As an outcome of the enormous surface-to-volume ratio, the adsorption/desorption of gas molecules can lead to dramatic modifications in electrical properties.[42,70] At exposure of individual ZnO NWs/NRs to ambient air in the temperature range of 25 to 150°C, mainly oxygen species are adsorbed on the surface by extracting free electrons from ZnO as follows:[5,74]

$$O_2(g) + e^- \rightarrow O_2^-(ads) \quad (7)$$

Extraction will lead to surface formation of an electron depletion region (EDR) of ZnO NWs/NRs and to the narrowing of the conduction channel through NWs/NRs, i.e. a rise of device resistance.[71] The observed tendency of an increase in gas response when rising the working temperature can be discussed based on the increased thermal energy of H_2 molecules and a reaction with adsorbed oxygen as follows:[5,75]

$$H_2(g) + \frac{1}{2}O_2^-(ads) \rightarrow H_2O(g) + e^- \quad (8)$$

This results in a narrowing of the EDR, leading to the decrease of device resistance. The excellent selectivity of individual ZnO NRs/NWs to H_2 gas can be explained based on the presence of Pt as contacts.[71] Pd or Pt due to the high catalytic effect, are known to contribute significantly to enhanced selectivity of hydrogen gas response.[76]

The integrated ZnO NRs/NWs synthesized at different temperatures show different gas responses, although they show practically the same diameter of the structure. From investigations of the structural and optical properties it was found that the higher temperature of ECD bath can result in a nanomaterial with better crystallinity. Therefore, the main cause of improved gas sensing performances can be the higher crystallinity of materials that results in the formation of contacts with higher quality. Also, it was observed that the CTA and AUT treatment can result in further improvements of gas sensing properties. This can be also explained in significantly improved crystallinity,[30] as well as in an efficient lowering of the concentration of Cl ions, as was demonstrated in previous works.[30,33,34] Also, as demonstrated by other studies, the doping of ZnO NWs with Cl may lead to metallic conduction that could negatively affect the gas detection properties of the devices.[23]

3.7. DFT Calculations: H_2 gas molecule interaction with ZnO (0001) and ZnO ($10\bar{1}0$) surfaces

In order to better understand the H_2 gas molecule interaction with ZnO NWs/NRs, DFT calculations on two active surfaces of ZnO were performed. Both Zn-terminated polar (0001) and nonpolar ($10\bar{1}0$) surfaces have been found very active surfaces and studied extensively for gas sensing and catalytic experiments.[77] Here, calculations on both these two surfaces to understand the H_2 gas sensing on ZnO NWs/NRs were done. Firstly, the modelled bulk wurtzite structure and calculated lattice parameters [a = b = 3.19571 Å, c = 5.14371 Å, α = β = 90°, γ = 120°] (see **Figure S6**) were found to match well with the experiments (a = b = 3.2490 Å, c = 5.2052 Å, α = β = 90°, and γ = 120°).[78] Calculated parameters of the lattice in this study are also in agreement with the earlier DFT computed results of Cook *et al.* (a = b = 3.1959 Å, c = 5.1585 Å, α = β = 90°, and γ = 120°).[79]

The macroscopic dipole of polar (0001) surface was quenched by removing one Zn atom from top and one oxygen atom from the bottom of the surface. The top layer of this ZnO (0001) surface consists of 3 Zn and 4 O atoms with the lattice parameters of a = 6.51 Å; b=6.51 Å. Hereby, total 6 atomic layers in the slab model and fixed bottom four layers to their bulk positions were considered, while the top 2 layers were allowed to relax. The surface energy with a value of 2.28 J.m-2, was calculated as described in the SI.

It was observed that after relaxation of the ZnO (0001) surface, the Zn-O bond in the top layers shrinks (Zn-O bond length changes to 1.85 and 1.92 Å from 1.88 and 1.94 Å respectively) forming a stronger bonding arrangement (see **Figure S7**). Next, a hydrogen molecule was placed closed to all the possible surface sites. It shows that the hydrogen molecule dissociates from the surface having an adsorption energy of -4.42 eV (see this value comparing **Figures 11(a, b))**. This spontaneous dissociation of the H_2 molecule was also found earlier for doped ZnO (0001) surfaces.[80] Next Bader charge analysis was performed to

quantify the charge transfer. It was noticed that -0.06 Bader charge is transferred to the molecule from the surface, as a result of surface-molecule interaction as shown in the charge density difference plot in **Figures 11(c, d)**. To further quantify the electronic structure changes, the electronic density of states (DOS) was calculated. The results show that there are considerable shifts in valence and conduction band states as a result of H_2 molecule interaction as shown in **Figures 11(e, f)**. Here, the Fermi energy changes from -2.735 eV for the ZnO (0001) surface to -1.352 eV after H_2 molecule adsorption over this surface.

In order to study the H_2 molecule interaction with the ZnO $(10\bar{1}0)$ surface, our recently modelled structure of the $(10\bar{1}0)$ surface was used,[81] where similar to earlier works[79,82] a termination (**Figure S8**) with a surface energy of 1.119 $J.m^{-2}$ was observed showing more stability compared to others.[79,82] The relaxed structure of the $(10\bar{1}0)$ surface is presented in **Figure S8**.

Here again, a H_2 molecule was placed closed to all possible sites of the surface. The results show that the molecule is physisorbed with a weak energy for adsorption of -0.258 eV, as can be seen in **Figure 12(a, b).** Bader charge analysis and charge density-difference plots show a very weak charge transfer to the molecule from the surface, as can be seen in **Figures 12(c, d)**. Moreover, electronic-DOS also suggests a weak interaction of the H_2 molecule as shown in **Figures 12(e, f),** with slight change in Fermi energy, as it values changes from -2.3761 for the ZnO $(10\bar{1}0)$ surface to -2.3655 when H_2 molecule is adsorbed over this surface. Overall, the results show that ZnO$(10\bar{1}0)$ interacts weakly with H_2 molecule, while the ZnO (0001) surface interacts strongly with an H_2 molecule.

4. CONCLUSION

ZnO NRs/NWs were electrodeposited on fluorine-doped tin oxide substrates at different temperatures of electrolyte solution, namely 70 °C, 80 °C and 90°C, to study its

influence on structural, chemical, optical and sensing performances of devices based on single nanostructures, integrated into nanosensor devices. The effects of post-growth relatively low temperature annealing/treatment and AUT at 150°C for 12 h on the morphology, structural properties, optical transmission, absorption, chemical composition, electronic structure and photoluminescence of ZnO NWs/NRs were investigated in detail. It was demonstrated that the use of higher temperatures during synthesis, as well as the exposure to post-growth annealing in water vapors can lead to improvements in the crystallinity of the electrodeposited ZnO-based nanomaterial. The individual ZnO NRs/NWs were integrated into micro- and nanodevices by the FIB/SEM technique for detailed detection tests. The experimentally obtained results demonstrate that hydrothermal annealing in water vapors of ZnO NRs/NWs is an efficient method to achieve high performances in the gas sensing of H_2 gas. At a temperature of 150 °C the gas response of ~ 380 to 100 ppm of H_2 gas detected. DFT calculations indicate that H_2 gas binds strongly with the ZnO (0001) surface and results in electronic bands shifts that are indicative of a better sensing capability of ZnO NRs/NWs.

■ ASSOCIATED CONTENT

Supporting Information: Additional information on DFT calculations of relaxed surface energy. Dynamic dependence of current density and cyclic voltammograms on FTO substrate, the EDX spectrum and the overview XPS spectra corresponding to ZnO NWs/NRs. UV response of individual ZnO nanowires. Figures of ZnO Bulk Structure, 2*2 supercell of the ZnO (0001) and $(10\bar{1}0)$ surfaces. The Supporting Information is available free of charge on the ACS Publications website at http://pubs.acs.org

■ AUTHOR INFORMATION

Corresponding Authors

*E-mails: oleg-lupan@mib.utm.md

akmishra@ddn.upes.ac.in; rasoul.khaledialidusti@ntnu.no

■ AUTHOR CONTRIBUTIONS

O.L. and Th.P. synthesized the nanomaterial and developed the synthesis-treatment methodology. L.K.O. and B.R.C. carried out XPS measurements and XPS data analysis. B.V. and O.L. carried out photoluminescence investigations and PL data analysis. O.L. and Th.P. carried out all Raman experiments and data discussion. O.L. and L.C. fitted a technology pathway for material integrations in the devices. N.M., V.P., O.L. performed the measurements of the detection characteristics of the nanomaterials and investigated the data. H.H. and L.C. investigated the TEM-HRTEM. O.L., N.M., S.H., R.A., H.K. and V.P. analyzed the experimental data/results, then the revised work. R.K.M. and A.K.M. accomplished the computational and DFT draft. A.K.M. performed and analyzed the computational results. O.L., N.M., S.H., V.P., L.K.O., B.R.C. and R.A. prepared the manuscript draft. O.L., Th.P., S.H., L.C. and R.A. accomplished the concept of this study and design. All gave the approval of the final version for manuscript to be submitted. This work was written based on all authors contributions. All of our co-authors reviewed the draft.

ACKNOWLEDGEMENTS

Dr. Lupan Oleg thanks Chimie-ParisTech PSL University for invited professor position in Paris. We acknowledge Dr. Delpech (Chimie-ParisTech) for studies on the Raman set-up. Dr. Mishra thanks the support from University Petroleum and Energy Studies from Dehradun. Leonard Siebert is acknowledge for fruitful discussions. This paper was partially supported by the Technical University of Moldova and the ANCD-NARD Grant No. 20.80009.5007.09 at TUM.

■ REFERENCES

(1) Kolmakov, A.; Moskovits, M. Chemical Sensing and Catalysis by One-Dimensional Metal-Oxide Nanostructures. *Annu. Rev. Mater. Res.* **2004,** *34*, 151-180.

(2) Lu, J. G.; Chang, P.; Fan, Z. Quasi-One-Dimensional Metal Oxide Materials—Synthesis, Properties and Applications. *Mater. Sci. Eng. R* **2006,** *52*, 49-91.

(3) Galstyan, V.; Kaur, N.; Zappa, D.; Núñez-Carmona, E.; Sberveglieri, V.; Comini, E. Chemical Gas Sensors Studied at SENSOR Lab, Brescia (Italy): From Conventional to Energy-Efficient and Biocompatible Composite Structures. *Sensors* **2020,** *20*, 579.

(4) Lupan, O.; Chai, G.; Chow, L. Novel hydrogen gas sensor based on single ZnO nanorod. *Microelectron. Eng.* **2008,** *85*, 2220-2225.

(5) Lupan, O.; Cretu, V.; Postica, V.; Ahmadi, M.; Cuenya, B. R.; Chow, L.; Tiginyanu, I.; Viana, B.; Pauporté, T.; Adelung, R. Silver-doped zinc oxide single nanowire multifunctional nanosensor with a significant enhancement in response. *Sens. Actuators B* **2016,** *223*, 893-903.

(6) Soci, C.; Zhang, A.; Xiang, B.; Dayeh, S. A.; Aplin, D. P. R.; Park, J.; Bao, X. Y.; Lo, Y. H.; Wang, D. ZnO Nanowire UV Photodetectors with High Internal Gain. *Nano Lett.* **2007,** *7*, 1003-1009.

(7) Lupan, O.; Postica, V.; Cretu, V.; Wolff, N.; Duppel, V.; Kienle, L.; Adelung, R. Single and networked CuO nanowires for highly sensitive p-type semiconductor gas sensor applications. *Phys. Status Solidi RRL* **2016,** *10*, 260-266.

(8) Lupan, O.; Postica, V.; Labat, F.; Ciofini, I.; Pauporté, T.; Adelung, R. Ultra-sensitive and selective hydrogen nanosensor with fast response at room temperature based on a single Pd/ZnO nanowire. *Sens. Actuators B* **2018,** *254*, 1259-1270.

(9) Lu, Y. J.; Shi, Z. F.; Shan, C. X.; Shen, D. Z. In *Nanoscale Semiconductor Lasers*; Elsevier, 2019.

(10) Lupan, O.; Guérin, V. M.; Tiginyanu, I. M.; Ursaki, V. V.; Chow, L.; Heinrich, H.; Pauporté, T. Well-aligned arrays of vertically oriented ZnO nanowires electrodeposited on ITO-coated glass and their integration in dye sensitized solar cells. *J. Photochem. Photobiol., A* **2010,** *211*, 65-73.

(11) Cui, Y.; Zhong, Z.; Wang, D.; Wang, W. U.; Lieber, C. M. High Performance Silicon Nanowire Field Effect Transistors. *Nano Lett.* **2003,** *3*, 149-152.

(12) Pauporté, T. In *Toward Functional Nanomaterials*; Springer, 2009.

(13) Wang, Z. M. *Toward functional nanomaterials*; Springer Science & Business Media, 2010.

(14) Pauporté, T.; Bataille, G.; Joulaud, L.; Vermersch, F. J. Well-Aligned ZnO Nanowire Arrays Prepared by Seed-Layer-Free Electrodeposition and Their Cassie−Wenzel Transition after Hydrophobization. *J. Phys. Chem. C* **2010,** *114*, 194-202.

(15) Singh, D. P. Synthesis and growth of ZnO nanowires. *Science of advanced materials* **2010,** *2*, 245-272.

(16) Drobek, M.; Kim, J.-H.; Bechelany, M.; Vallicari, C.; Julbe, A.; Kim, S. S. MOF-Based Membrane Encapsulated ZnO Nanowires for Enhanced Gas Sensor Selectivity. *ACS Appl. Mater. Interfaces* **2016,** *8*, 8323-8328.

(17) Drobek, M.; Kim, J.-H.; Bechelany, M.; Vallicari, C.; Leroy, E.; Julbe, A.; Kim, S. S. Design and Fabrication of Highly Selective H_2 Sensors Based on SIM-1 Nanomembrane-Coated ZnO Nanowires. *Sens. Actuators B* **2018,** *264*, 410-418.

(18) Weber, M.; Kim, J.-H.; Lee, J.-H.; Kim, J.-Y.; Iatsunskyi, I.; Coy, E.; Drobek, M.; Julbe, A.; Bechelany, M.; Kim, S. S. High-Performance Nanowire Hydrogen Sensors

by Exploiting the Synergistic Effect of Pd Nanoparticles and Metal–Organic Framework Membranes. *ACS Appl. Mater. Interfaces* **2018,** *10*, 34765-34773.

(19) Weber, M.; Kim, J.-Y.; Lee, J.-H.; Kim, J.-H.; Iatsunskyi, I.; Coy, E.; Miele, P.; Bechelany, M.; Kim, S. S. Highly Efficient Hydrogen Sensors Based on Pd Nanoparticles Supported on Boron Nitride Coated ZnO Nanowires. *J. Mater. Chem. A* **2019,** *7*, 8107-8116.

(20) Pauporté, T.; Cortès, R.; Froment, M.; Beaumont, B.; Lincot, D. Electrocrystallization of Epitaxial Zinc Oxide onto Gallium Nitride. *Chem. Mater.* **2002,** *14*, 4702-4708.

(21) Pauporté, T.; Lincot, D. Hydrogen Peroxide Oxygen Precursor for Zinc Oxide Electrodeposition I. Deposition in Perchlorate Medium. *J. Electrochem. Soc.* **2001,** *148*, C310.

(22) Pauporté, T.; Lupan, O.; Postica, V.; Hoppe, M.; Chow, L.; Adelung, R. Al-Doped ZnO Nanowires by Electrochemical Deposition for Selective VOC Nanosensor and Nanophotodetector. *Phys. Status Solidi (a)* **2018,** *215*, 1700824.

(23) Wang, F.; Seo, J.-H.; Li, Z.; Kvit, A. V.; Ma, Z.; Wang, X. Cl-Doped ZnO Nanowires with Metallic Conductivity and Their Application for High-Performance Photoelectrochemical Electrodes. *ACS Appl. Mater. Interfaces* **2014,** *6*, 1288-1293.

(24) Lupan, O.; Postica, V.; Adelung, R.; Labat, F.; Ciofini, I.; Schürmann, U.; Kienle, L.; Chow, L.; Viana, B.; Pauporté, T. Functionalized Pd/ZnO Nanowires for Nanosensors. *Phys. Status Solidi RRL* **2018,** *12*, 1700321.

(25) Lupan, O.; Pauporté, T.; Viana, B.; Aschehoug, P. Electrodeposition of Cu-doped ZnO nanowire arrays and heterojunction formation with p-GaN for color tunable light emitting diode applications. *Electrochim. Acta* **2011,** *56*, 10543-10549.

(26) Lupan, O.; Pauporte, T.; Lee, C. Synthesis and gas sensor applications of nanostructured ZnO grown at low temperatures. *Turk. J. Phys.* **2014,** *38*, 399-419.

(27) Lupan, O.; Postica, V.; Pauporté, T.; Hoppe, M.; Adelung, R. UV nanophotodetectors: A case study of individual Au-modified ZnO nanowires. *Sens. Actuators A* **2019,** *296*, 400-408.

(28) Lupan, O.; Postica, V.; Pauporté, T.; Viana, B.; Terasa, M.-I.; Adelung, R. Room temperature gas nanosensors based on individual and multiple networked Au-modified ZnO nanowires. *Sens. Actuators B* **2019,** *299*, 126977.

(29) Lupan, O.; Postica, V.; Wolff, N.; Su, J.; Labat, F.; Ciofini, I.; Cavers, H.; Adelung, R.; Polonskyi, O.; Faupel, F.; Kienle, L.; Viana, B.; Pauporté, T. Low-Temperature Solution Synthesis of Au-Modified ZnO Nanowires for Highly Efficient Hydrogen Nanosensors. *ACS Appl. Mater. Interfaces* **2019,** *11*, 32115-32126.

(30) Lupan, O.; Pauporté, T. Hydrothermal treatment for the marked structural and optical quality improvement of ZnO nanowire arrays deposited on lightweight flexible substrates. *J. Cryst. Growth* **2010,** *312*, 2454-2458.

(31) Kim, J.-W.; Porte, Y.; Ko, K. Y.; Kim, H.; Myoung, J.-M. Micropatternable Double-Faced ZnO Nanoflowers for Flexible Gas Sensor. *ACS Appl. Mater. Interfaces* **2017,** *9*, 32876-32886.

(32) Tian, W.; Zhang, C.; Zhai, T.; Li, S.-L.; Wang, X.; Liu, J.; Jie, X.; Liu, D.; Liao, M.; Koide, Y.; Golberg, D.; Bando, Y. Flexible Ultraviolet Photodetectors with Broad Photoresponse Based on Branched ZnS-ZnO Heterostructure Nanofilms. *Adv. Mater.* **2014,** *26*, 3088-3093.

(33) Lupan, O.; Pauporté, T.; Chow, L.; Viana, B.; Pellé, F.; Ono, L. K.; Roldan Cuenya, B.; Heinrich, H. Effects of annealing on properties of ZnO thin films prepared by electrochemical deposition in chloride medium. *Appl. Surf. Sci.* **2010,** *256*, 1895-1907.

(34) Lupan, O.; Pauporté, T.; Tiginyanu, I. M.; Ursaki, V. V.; Şontea, V.; Ono, L. K.; Cuenya, B. R.; Chow, L. Comparative study of hydrothermal treatment and thermal

annealing effects on the properties of electrodeposited micro-columnar ZnO thin films. *Thin Solid Films* **2011,** *519*, 7738-7749.
(35) Lupan, O.; Pauporté, T.; Ursaki, V. V.; Tiginyanu, I. M. Highly luminescent columnar ZnO films grown directly on n-Si and p-Si substrates by low-temperature electrochemical deposition. *Opt. Mater.* **2011,** *33*, 914-919.
(36) Peulon, S. Mechanistic Study of Cathodic Electrodeposition of Zinc Oxide and Zinc Hydroxychloride Films from Oxygenated Aqueous Zinc Chloride Solutions. *J. Electrochem. Soc.* **1998,** *145*, 864.
(37) Kinoshita, K. *Electrochemical oxygen technology*; John Wiley & Sons, 1992.
(38) Goux, A.; Pauporté, T.; Lincot, D. Oxygen reduction reaction on electrodeposited zinc oxide electrodes in KCl solution at 70°C. *Electrochim. Acta* **2006,** *51*, 3168-3172.
(39) Lupan, O.; Pauporté, T.; Tiginyanu, I. M.; Ursaki, V. V.; Heinrich, H.; Chow, L. Optical properties of ZnO nanowire arrays electrodeposited on n- and p-type Si(111): Effects of thermal annealing. *Mater. Sci. Eng. B* **2011,** *176*, 1277-1284.
(40) Lupan, O.; Chow, L.; Chai, G.; Roldan, B.; Naitabdi, A.; Schulte, A.; Heinrich, H. Nanofabrication and characterization of ZnO nanorod arrays and branched microrods by aqueous solution route and rapid thermal processing. *Mater. Sci. Eng.: B* **2007,** *145*, 57-66.
(41) Lupan, O.; Chow, L.; Chai, G.; Heinrich, H. Fabrication and characterization of Zn–ZnO core–shell microspheres from nanorods. *Chem. Phys. Lett.* **2008,** *465*, 249-253.
(42) Lupan, O.; Postica, V.; Wolff, N.; Polonskyi, O.; Duppel, V.; Kaidas, V.; Lazari, E.; Ababii, N.; Faupel, F.; Kienle, L.; Adelung, R. Localized Synthesis of Iron Oxide Nanowires and Fabrication of High Performance Nanosensors Based on a Single Fe_2O_3 Nanowire. *Small* **2017,** *13*, 1602868.
(43) Cretu, V.; Postica, V.; Mishra, A. K.; Hoppe, M.; Tiginyanu, I.; Mishra, Y. K.; Chow, L.; de Leeuw, N. H.; Adelung, R.; Lupan, O. Synthesis, characterization and DFT studies of zinc-doped copper oxide nanocrystals for gas sensing applications. *J. Mater. Chem. A* **2016,** *4*, 6527-6539.
(44) Perdew, J. P.; Burke, K.; Ernzerhof, M. Generalized gradient approximation made simple. *Phys. Rev. Lett.* **1996,** *77*, 3865.
(45) Blöchl, P. E. Projector augmented-wave method. *Phys. Rev. B* **1994,** *50*, 17953-17979.
(46) Kresse, G.; Joubert, D. From ultrasoft pseudopotentials to the projector augmented-wave method. *Phys. Rev. B* **1999,** *59*, 1758-1775.
(47) Kresse, G.; Furthmüller, J. Efficiency of ab-initio total energy calculations for metals and semiconductors using a plane-wave basis set. *Comput. Mater. Sci.* **1996,** *6*, 15-50.
(48) Press, W. H.; Flannery, B. P.; Teukolsky, S. A.; Vetterling, W. T. Numerical recipes: The art of scientific computing((Book)). *Cambridge and New York, Cambridge University Press, 1986, 839* **1986**.
(49) Monkhorst, H. J.; Pack, J. D. Special points for Brillouin-zone integrations. *Phys. Rev. B* **1976,** *13*, 5188.
(50) Grimme, S. Semiempirical GGA‐type density functional constructed with a long‐range dispersion correction. *J. Comput. Chem.* **2006,** *27*, 1787-1799.
(51) Tak, Y.; Yong, K. Controlled Growth of Well-Aligned ZnO Nanorod Array Using a Novel Solution Method. *J. Phys. Chem. B* **2005,** *109*, 19263-19269.
(52) Guillemin, S.; Consonni, V.; Appert, E.; Puyoo, E.; Rapenne, L.; Roussel, H. Critical Nucleation Effects on the Structural Relationship Between ZnO Seed Layer and Nanowires. *J. Phys. Chem. C* **2012,** *116*, 25106-25111.
(53) Lupan, O.; Chai, G.; Chow, L.; Emelchenko, G. A.; Heinrich, H.; Ursaki, V. V.; Gruzintsev, A. N.; Tiginyanu, I. M.; Redkin, A. N. Ultraviolet photoconductive sensor based on single ZnO nanowire. *Phys. Status Solidi (a)* **2010,** *207*, 1735-1740.

(54) Lupan, O.; Chow, L.; Chai, G.; Roldan Cuenya, B.; Naitabdi, A.; Schulte, A.; Heinrich, H. Nanofabrication and characterization of ZnO nanorod arrays and branched microrods by aqueous solution route and rapid thermal processing. *Materials Science and Engineering B* **2007,** *145*, 57-66.
(55) Nefedov, V. I.; Salyn, Y. V.; Leonhardt, G.; Scheibe, R. Comparison of Different Spectrometers and Charge Corrections Used in X-Ray Photoelectron-Spectroscopy. *Journal of Electron Spectroscopy and Related Phenomena* **1977,** *10*, 121-124.
(56) Kawase, K.; Tanimura, J.; Kurokawa, H.; Wakao, K.; Inone, M.; Umeda, H.; Teramoto, A. XPS study of H-terminated silicon surface under inert gas and UHV annealing. *Journal of the Electrochemical Society* **2005,** *152*, G163-G167.
(57) Strohmeier, B. R.; Hercules, D. M. Surface Spectroscopic Characterization of the Interaction between Zinc Ions and Gamma-Alumina. *Journal of Catalysis* **1984,** *86*, 266-279.
(58) Jeong, S. H.; Yoo, D. G.; Kim, D. Y.; Lee, N. E.; Boo, J. H. Physical properties and etching characteristics of metal (Al, Ag, Li) doped ZnO films grown by RF magnetron sputtering. *Thin Solid Films* **2008,** *516*, 6598-6603.
(59) Tanaka, K.; Miyahara, K.; Toyoshima, I. Adsorption of Co2 on Tio2 and Pt/Tio2 Studied by X-Ray Photoelectron-Spectroscopy and Auger-Electron Spectroscopy. *Journal of Physical Chemistry* **1984,** *88*, 3504-3508.
(60) Carley, A. F.; Hawkins, G.; Read, S.; Roberts, M. W. Reactions of co-adsorbed carbon dioxide and dioxygen at the Mg(0001) surface at low temperatures. *Topics in Catalysis* **1999,** *8*, 243-248.
(61) Onishi, H.; Egawa, C.; Aruga, T.; Iwasawa, Y. Adsorption of Na Atoms and Oxygen-Containing Molecules on Mgo(100) and (111) Surfaces. *Surface Science* **1987,** *191*, 479-491.
(62) Lupan, O.; Emelchenko, G. A.; Ursaki, V. V.; Chai, G.; Redkin, A. N.; Gruzintsev, A. N.; Tiginyanu, I. M.; Chow, L.; Ono, L. K.; Roldan Cuenya, B.; Heinrich, H.; Yakimov, E. E. Synthesis and characterization of ZnO nanowires for nanosensor applications. *Mater. Res. Bull.* **2010,** *45*, 1026-1032.
(63) Armelao, L.; Fabrizio, M.; Gialanella, S.; Zordan, F. Sol-gel synthesis and characterisation of ZnO-based nanosystems. *Thin Solid Films* **2001,** *394*, 90-96.
(64) Liqiang, J.; Dejun, W.; Baiqi, W.; Shudan, L.; Baifu, X.; Honggang, F.; Jiazhong, S. Effects of noble metal modification on surface oxygen composition, charge separation and photocatalytic activity of ZnO nanoparticles. *Journal of Molecular Catalysis A: Chemical* **2006,** *244*, 193-200.
(65) Wang, F.; He, H.; Ye, Z.; Zhu, L.; Tang, H.; Zhang, Y. Raman scattering and photoluminescence of quasi-aligned ternary ZnCdO nanorods. *J. Phys. D. Appl. Phys.* **2005,** *38*, 2919-2922.
(66) Lupan, O.; Pauporté, T.; Viana, B.; Tiginyanu, I. M.; Ursaki, V. V.; Cortès, R. Epitaxial Electrodeposition of ZnO Nanowire Arrays on p-GaN for Efficient UV-Light-Emitting Diode Fabrication. *ACS Appl. Mater. Interfaces* **2010,** *2*, 2083-2090.
(67) Yang, J.; Liu, X.; Yang, L.; Wang, Y.; Zhang, Y.; Lang, J.; Gao, M.; Feng, B. Effect of annealing temperature on the structure and optical properties of ZnO nanoparticles. *J. Alloys Compd.* **2009,** *477*, 632-635.
(68) Postica, V.; Hoppe, M.; Gröttrup, J.; Hayes, P.; Röbisch, V.; Smazna, D.; Adelung, R.; Viana, B.; Aschehoug, P.; Pauporté, T.; Lupan, O. Morphology dependent UV photoresponse of Sn-doped ZnO microstructures. *Solid State Sci.* **2017,** *71*, 75-86.
(69) Janotti, A.; Van de Walle, C. G. Native point defects in ZnO. *Phys. Rev. B* **2007,** *76*, 165202.

(70) Schütt, F.; Postica, V.; Adelung, R.; Lupan, O. Single and Networked ZnO–CNT Hybrid Tetrapods for Selective Room-Temperature High-Performance Ammonia Sensors. *ACS Appl. Mater. Interfaces* **2017,** *9*, 23107-23118.
(71) Hoppe, M.; Lupan, O.; Postica, V.; Wolff, N.; Duppel, V.; Kienle, L.; Tiginyanu, I.; Adelung, R. $ZnAl_2O_4$-Functionalized Zinc Oxide Microstructures for Highly Selective Hydrogen Gas Sensing Applications. *Phys. Status Solidi (a)* **2018,** *215*, 1700772.
(72) Postica, V.; Gröttrup, J.; Adelung, R.; Lupan, O.; Mishra, A. K.; de Leeuw, N. H.; Ababii, N.; Carreira, J. F. C.; Rodrigues, J.; Sedrine, N. B. Multifunctional Materials: A Case Study of the Effects of Metal Doping on ZnO Tetrapods with Bismuth and Tin Oxides. *Adv. Funct. Mater.* **2017,** *27*, 1604676.
(73) Liu, J.; Wu, W.; Bai, S.; Qin, Y. Synthesis of High Crystallinity ZnO Nanowire Array on Polymer Substrate and Flexible Fiber-Based Sensor. *ACS Appl. Mater. Interfaces* **2011,** *3*, 4197-4200.
(74) Kolmakov, A.; Zhang, Y.; Cheng, G.; Moskovits, M. Detection of CO and O_2 Using Tin Oxide Nanowire Sensors. *Adv. Mater.* **2003,** *15*, 997-1000.
(75) Chang, J. F.; Kuo, H. H.; Leu, I. C.; Hon, M. H. The effects of thickness and operation temperature on ZnO:Al thin film CO gas sensor. *Sens. Actuators B* **2002,** *84*, 258-264.
(76) Das, S. N.; Kar, J. P.; Choi, J.-H.; Lee, T. I.; Moon, K.-J.; Myoung, J.-M. Fabrication and Characterization of ZnO Single Nanowire-Based Hydrogen Sensor. *J. Phys. Chem. C* **2010,** *114*, 1689-1693.
(77) Nyberg, M.; Nygren, M. A.; Pettersson, L. G. M.; Gay, D. H.; Rohl, A. L. Hydrogen Dissociation on Reconstructed ZnO Surfaces. *J. Phys. Chem.* **1996,** *100*, 9054-9063.
(78) Sawada, H.; Wang, R.; Sleight, A. W. An electron density residual study of zinc oxide. *J. Solid State Chem.* **1996,** *122*, 148-150.
(79) Cooke, D. J.; Marmier, A.; Parker, S. C. Surface Structure of $(10\bar{1}0)$ and $(11\bar{2}0)$ Surfaces of ZnO with Density Functional Theory and Atomistic Simulation. *J. Phys. Chem. B* **2006,** *110*, 7985-7991.
(80) Lupan, O.; Postica, V.; Gröttrup, J.; Mishra, A. K.; de Leeuw, N. H.; Carreira, J. F. C.; Rodrigues, J.; Ben Sedrine, N.; Correia, M. R.; Monteiro, T.; Cretu, V.; Tiginyanu, I.; Smazna, D.; Mishra, Y. K.; Adelung, R. Hybridization of Zinc Oxide Tetrapods for Selective Gas Sensing Applications. *ACS Appl. Mater. Interfaces* **2017,** *9*, 4084-4099.
(81) Lupan, C.; Khaledialidusti, R.; Mishra, A. K.; Postica, V.; Terasa, M.-I.; Magariu, N.; Pauporté, T.; Viana, B.; Drewes, J.; Vahl, A.; Faupel, F.; Adelung, R. Pd-Functionalized ZnO:Eu Columnar Films for Room-Temperature Hydrogen Gas Sensing: A Combined Experimental and Computational Approach. *ACS Appl. Mater. Interfaces* **2020,** *12*, 24951-24964.
(82) Wander, A.; Harrison, N. M. An ab-initio study of ZnO (1120). *Surf. Sci.* **2000,** *468*, L851-L855.

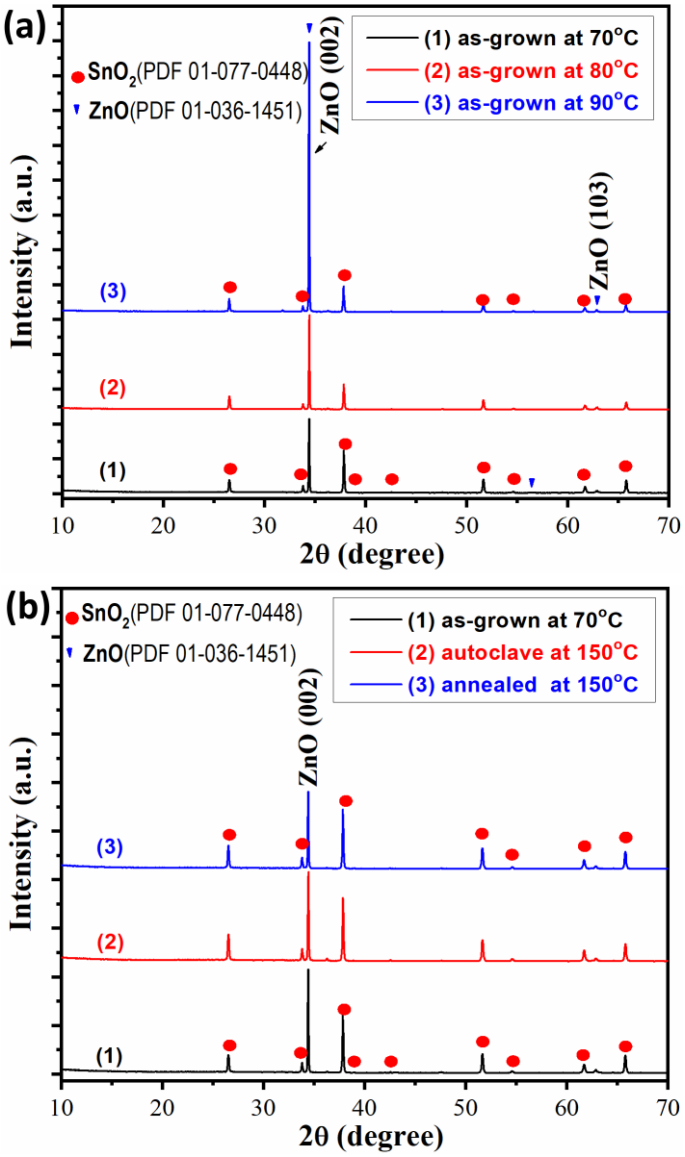

Figure 1. XRD diffractograms of ZnO NRs/NWs electrodeposited at: (a) 70 °C, 80 °C, and 90 °C. (b) at 70 °C and CTA 150 °C in air and hydrothermal treated-HT at 150 °C in autoclave with H_2O vapors in the ambient.

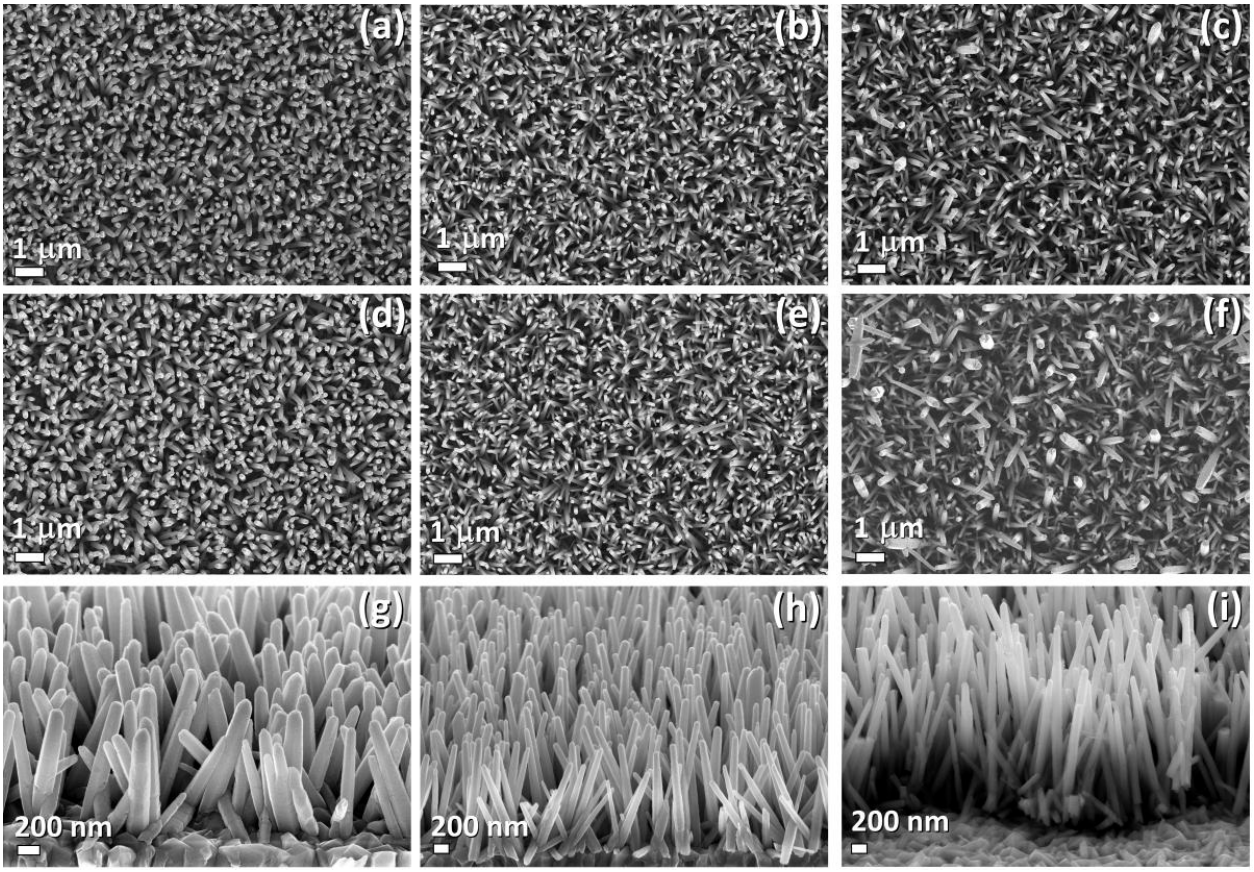

Figure 2. SEM images of electrodeposited ZnO NRs/NWs (top view) initially and after post-synthesis treatment/annealing: (a) as-grown at 70°C (2.5 h); (b) as-grown at 80 °C (2.5 h); (c) as-grown at 90°C (2.5 h); (d) grown at 70°C (2.5 h) and hydrothermal treated at 150 °C in H_2O vapor ambient, 12 h; (e) grown at 80°C (2.5 h) and AUT-HT at 150°C, 12 h in an autoclave; (f) grown at 90 °C (2.5 h) and treated- AUT-HT at 150°C, 12 h; (g) 65°-tilted-view of image (d); (h) 65°-tilted-view of image (e); (i) 65°-tilted-view of image (f).

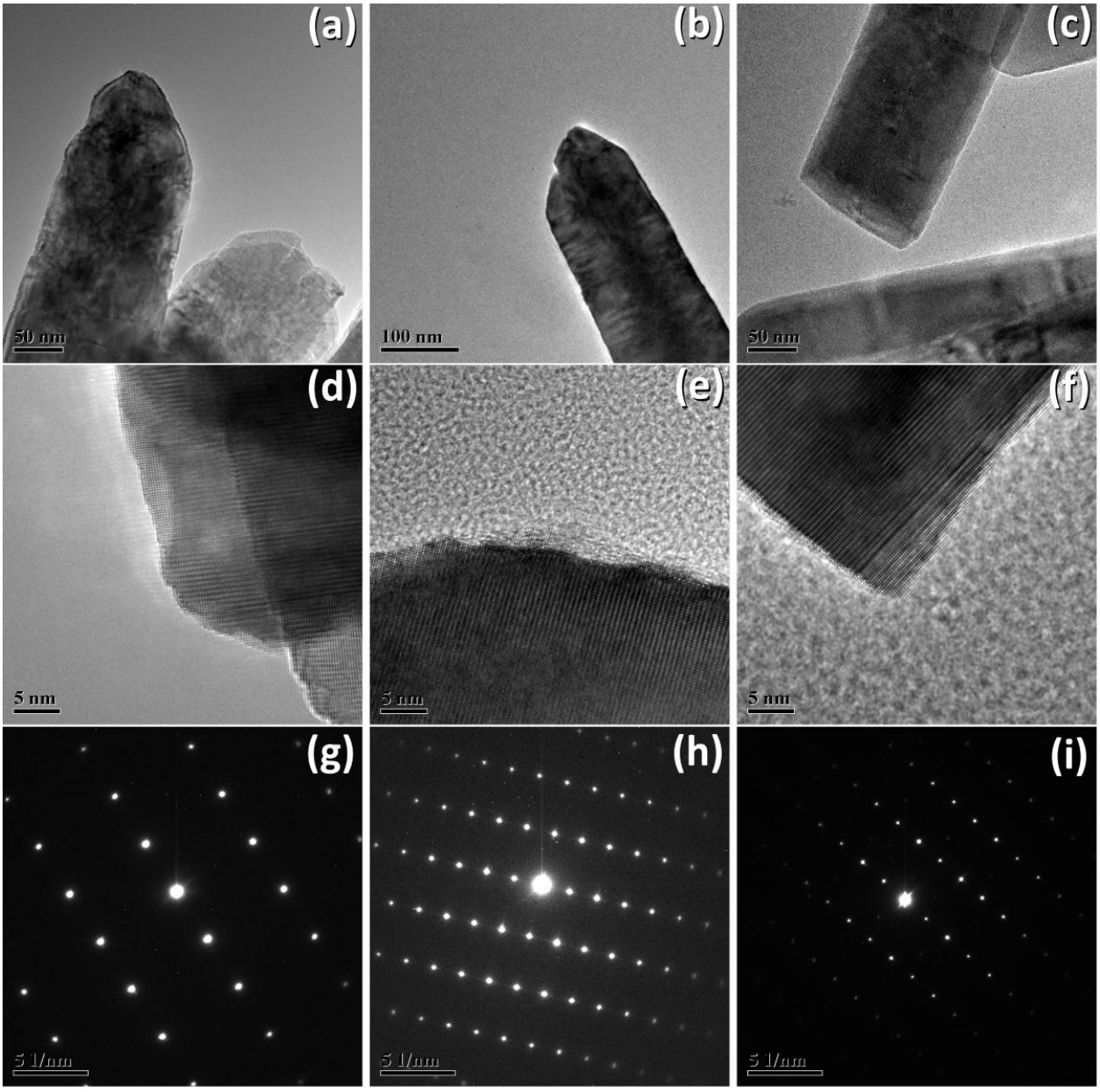

Figure 3. TEM of ZnO NRs/NWs grown by electrodeposition: (a) as-grown at 70 °C (2.5 h); (b) grown at 80 °C (2.5 h); (c) grown at 90 °C (2.5 h) and treated AUT-HT at 150 °C, 12 h in an autoclave. HRTEM of ECD ZnO NRs/NWs: (d) as-grown at 70 °C(2.5 h); (e) grown at 80 °C (2.5 h); (f) grown at 90 °C (2.5 h) and treated- AUT-HT at 150 °C, 12 h. Typical SAED patterns of ZnO NRs/NWs grown by electrodeposition at: (g) 70 °C, (h) 80 °C and (i) 90 °C.

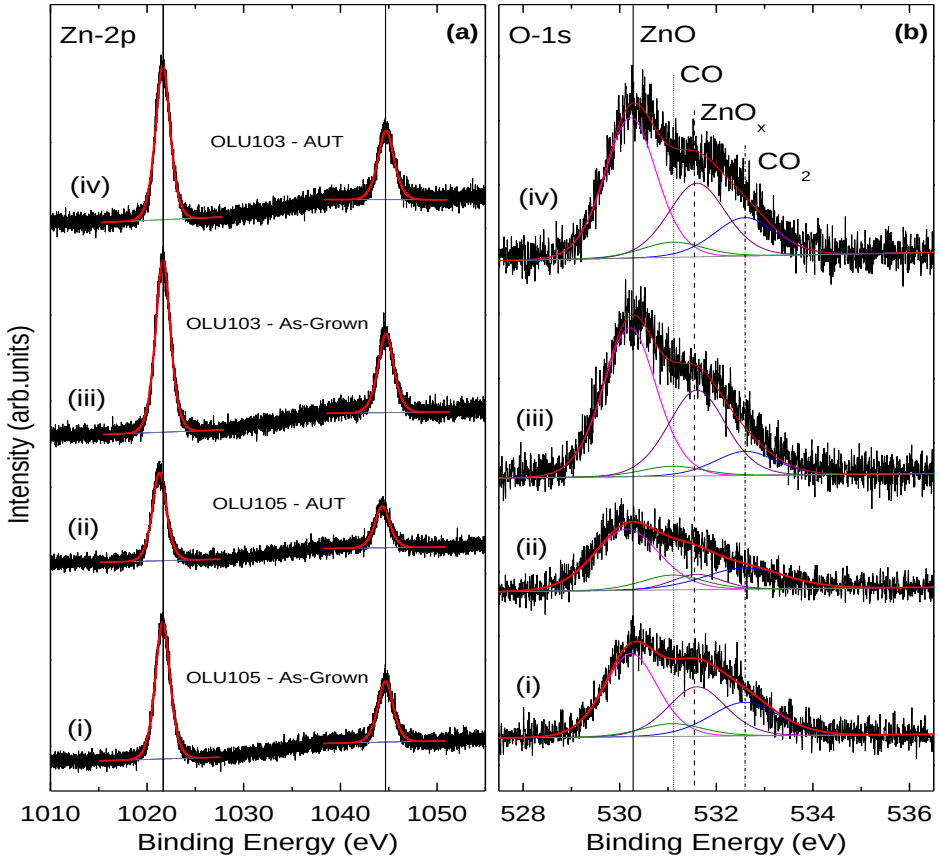

Figure 4. XPS spectra (Al-K_α = 1486.6 eV) investigated to the (a) Zn-2p and (b) O-1s core level regions of ZnO NWs synthesized on FTO/glass substrates. The vertical lines in (b) indicate the binding energies of O-1s in stoichiometric and defective ZnO, as well as in adventitious CO and CO_2.

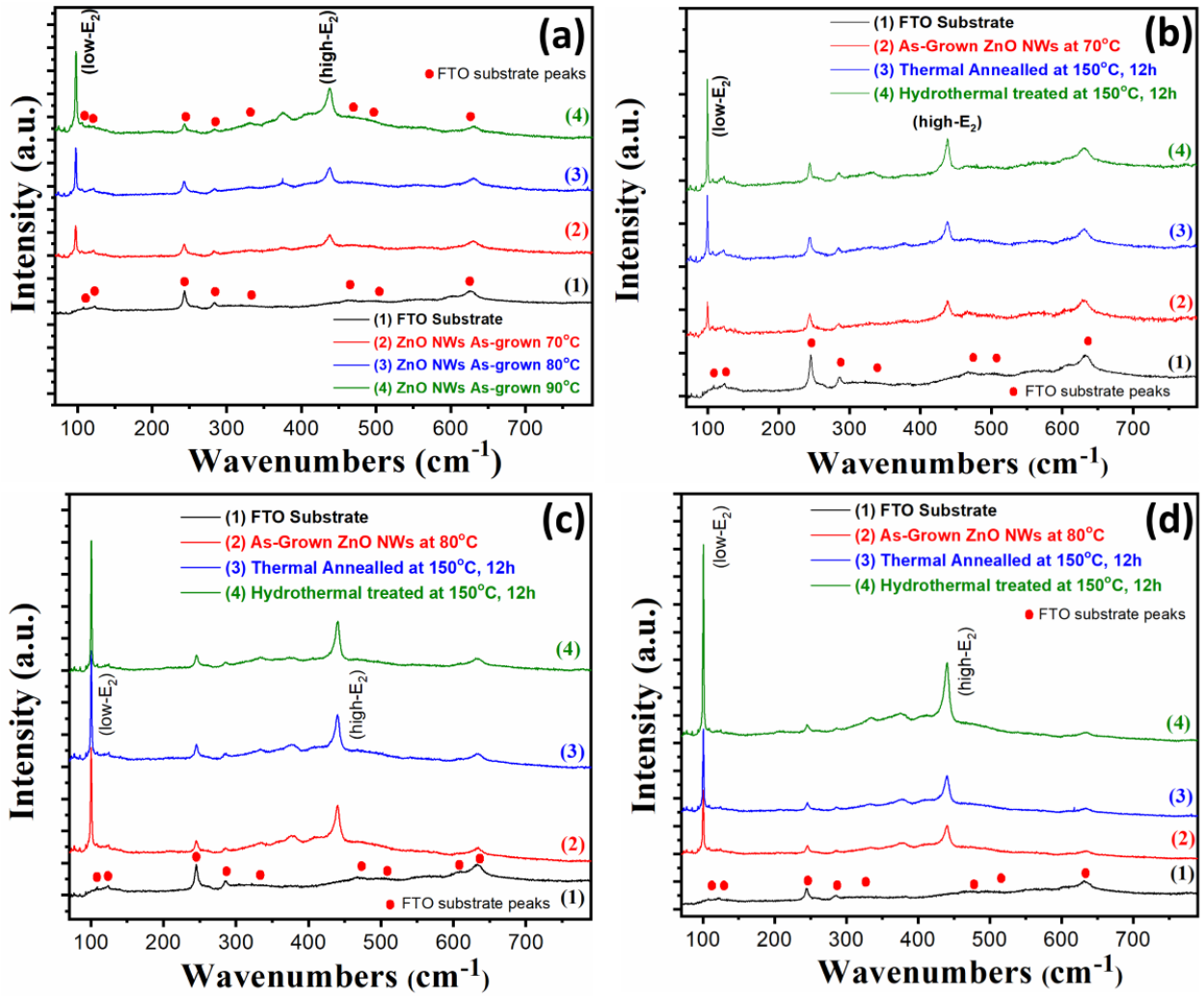

Figure 5. Raman spectra for initially and annealed/treated-HT ZnO nanorod/nanowire arrays on FTO substrate measured at room temperature: (a) comparison of samples grown at different temperatures 70 °C, 80 °C, and 90 °C; (b) comparison of samples grown at 70 °C and subjected to different post-growth treatments; (c) comparison of samples grown at 80 °C; and (d) comparison of samples grown at 90 °C and subjected to different post-growth treatments.

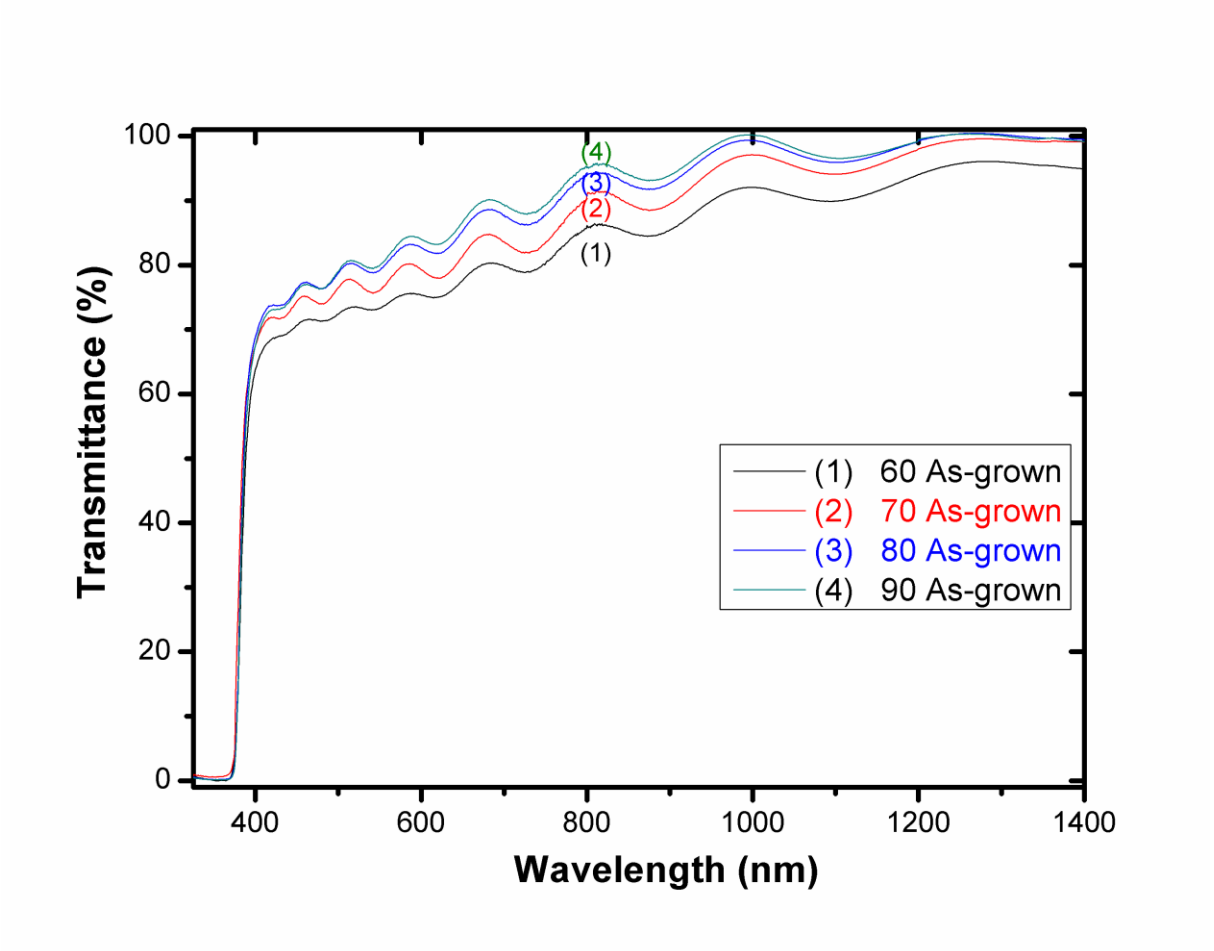

Figure 6. Transmission spectra of as-synthesized ZnO NRs/NWs electrochemically grown on FTO substrates at 60 °C, 70 °C, 80 °C, and 90 °C.

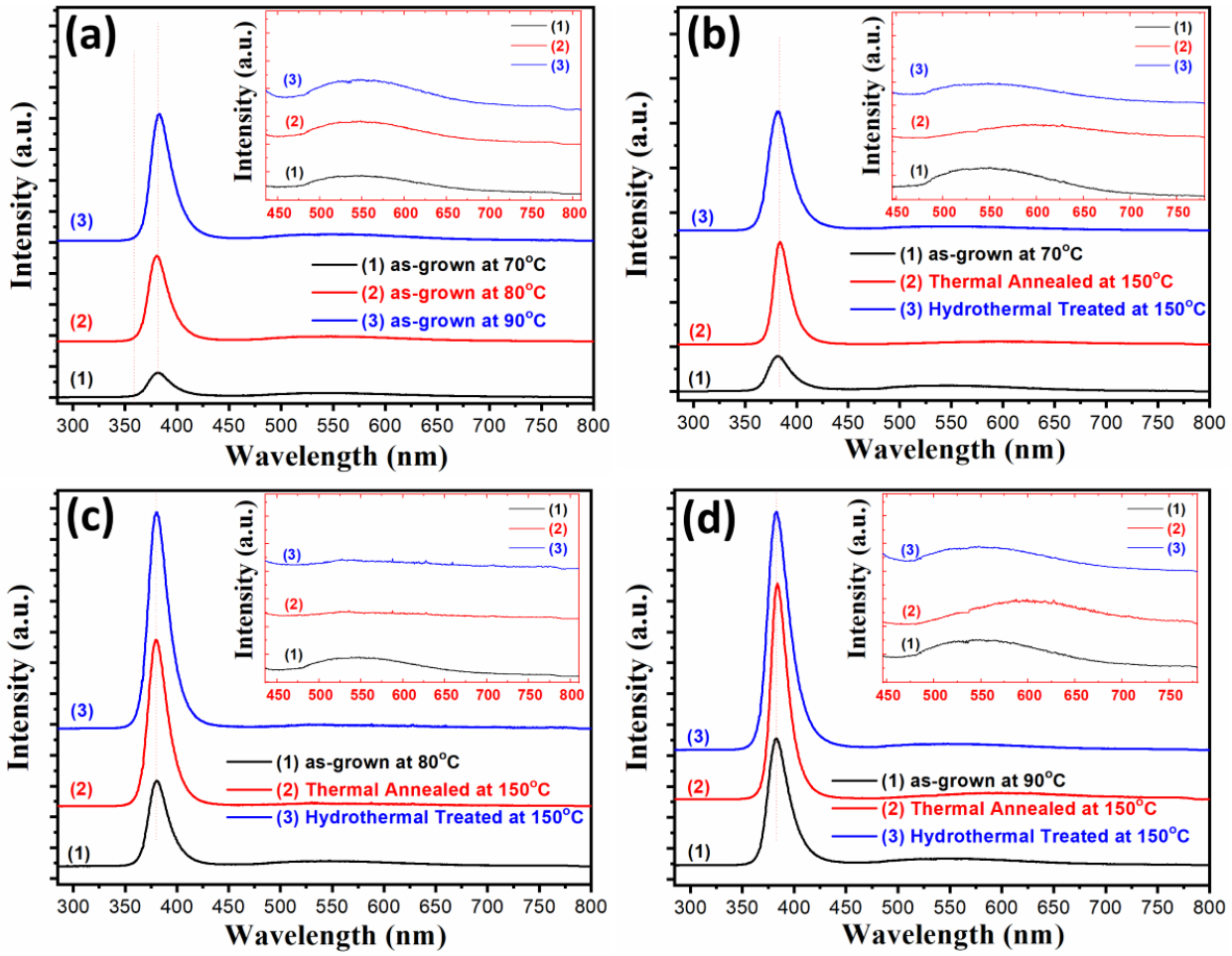

Figure 7. PL room-temperature spectra for as-synthesized and annealed/treated-HT ZnO NRs/NWs arrays on FTO: (a) comparison of samples grown at various temperatures as indicated on graph; (b) comparison of samples obtained at 70 °C and subjected to different post-growth treatments; (c) comparison of samples grown at 80 °C; and (d) comparison of samples grown at 90 °C and subjected to different post-growth annealing/treatments-HT. Insert represents zoom-in visible regions of the same photoluminescence spectra.

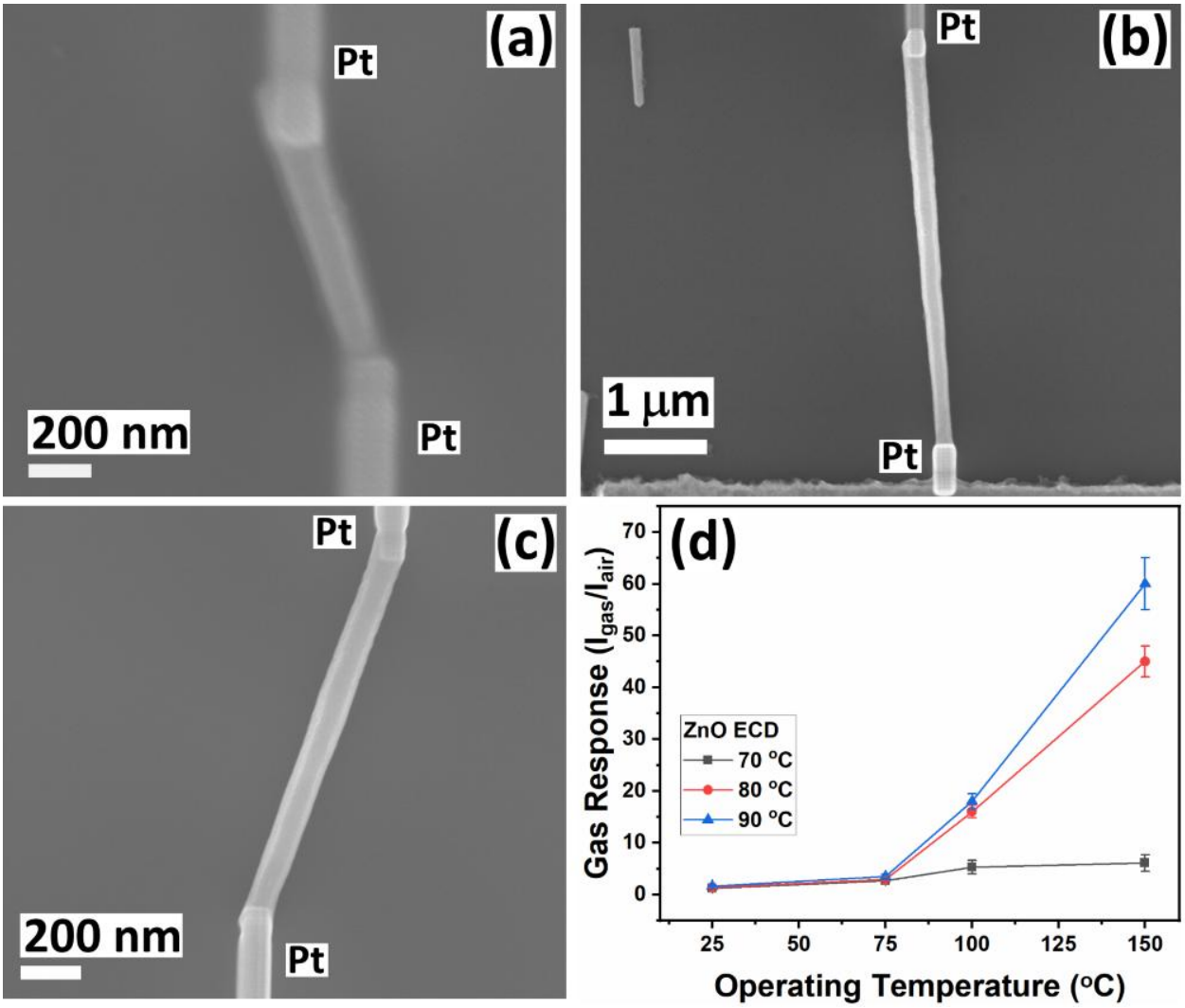

Figure 8. SEM images of microdevices/sensors constructed on individual ZnO NRs/NWs synthesized at: (a) 70 °C, (b) 80 °C and (c) 90 °C. (d) Response vs working temperature of devices to 100 ppm of hydrogen.

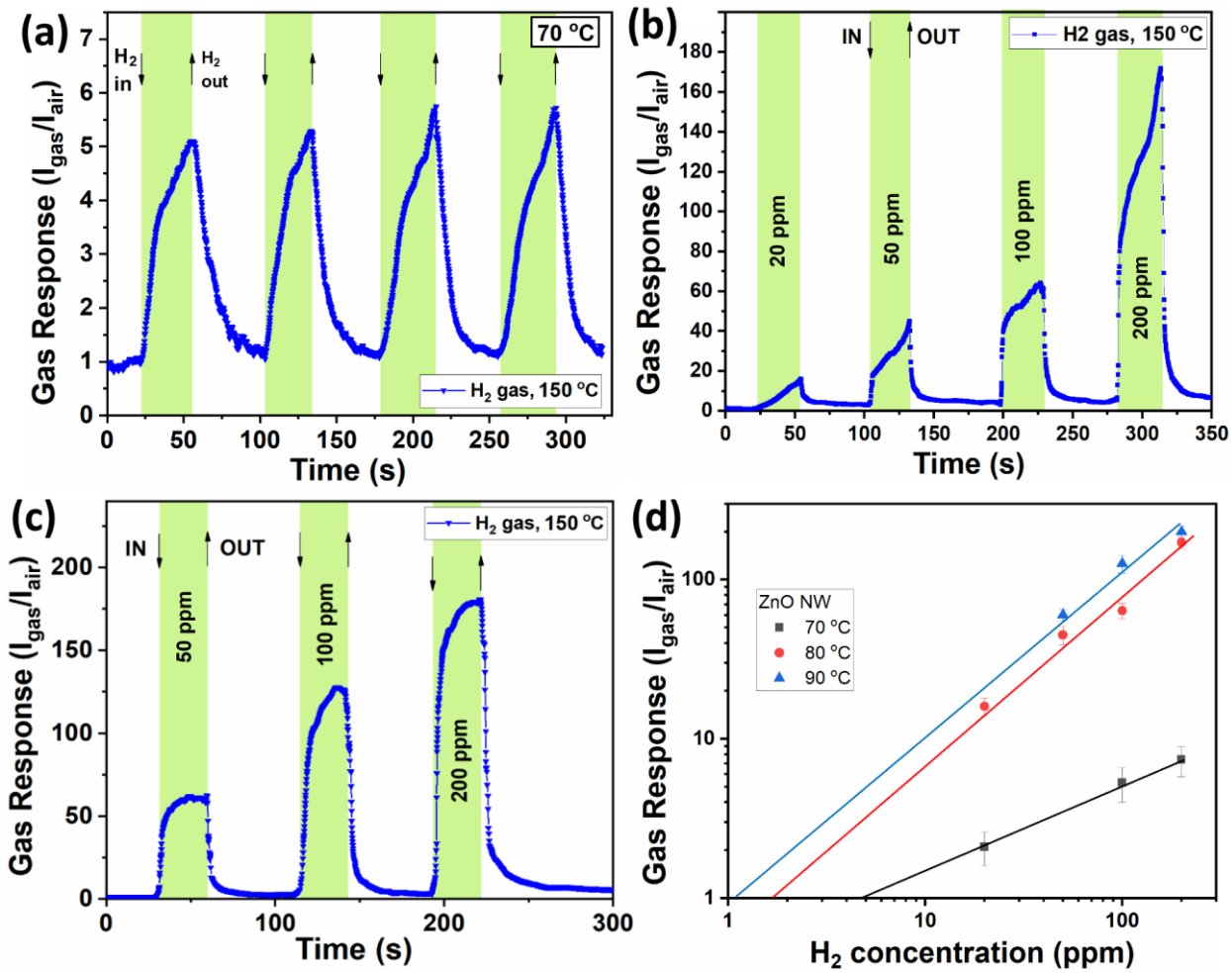

Figure 9. (a) Dynamic gas response at 150 °C of individual ZnO NRs/NWs synthesized at 70 °C to multiple exposures of H_2 gas with 100 ppm as well as to different concentrations of hydrogen gas for a single ZnO NRs/NWs synthesized at: (b) 80 °C and (c) 90 °C. (d) Dependence of gas response on gas H_2 concentration at 150 °C for individual ZnO NRs/NWs synthesized at 70 °C, 80 °C and 90 °C.

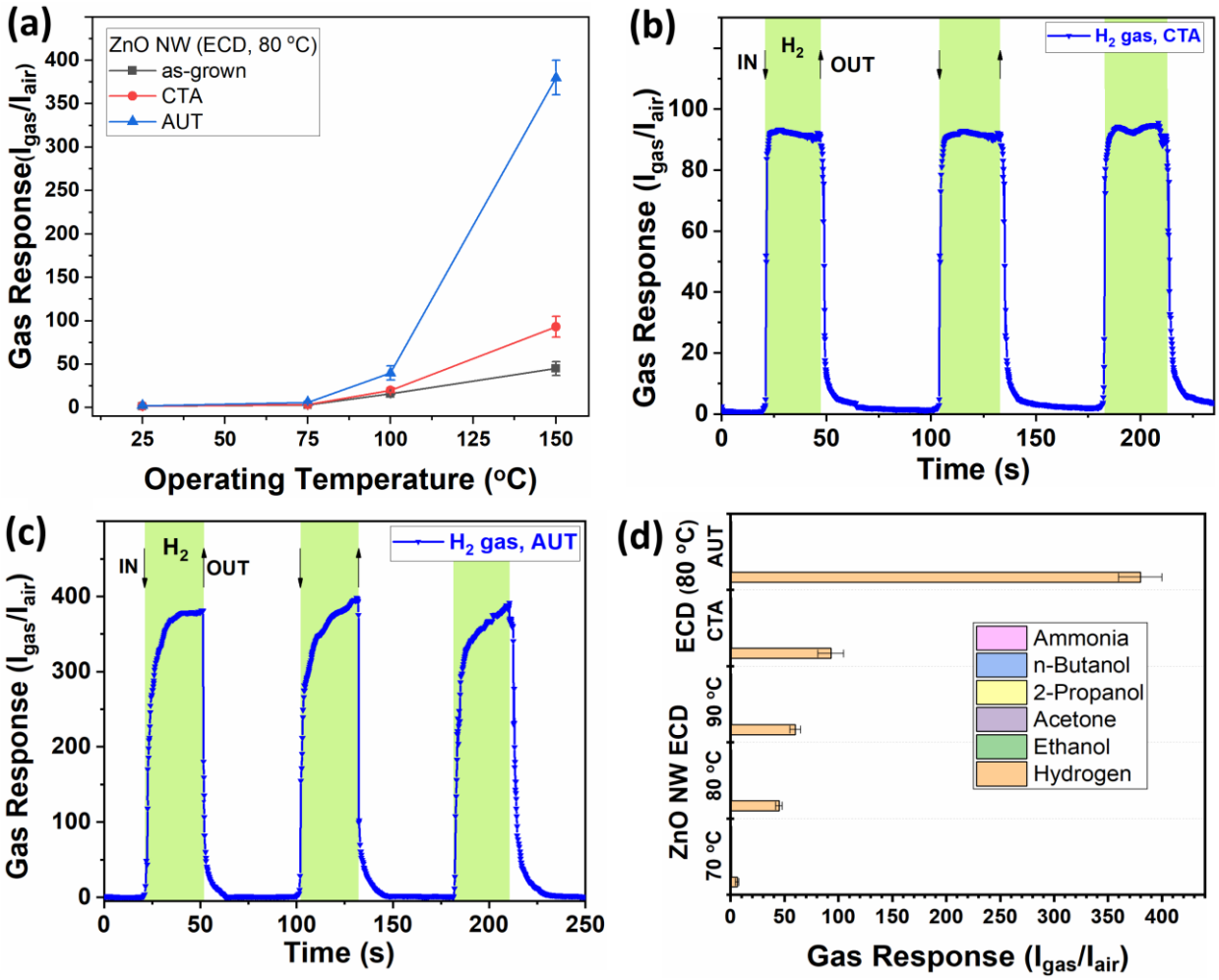

Figure 10. (a) Response vs working temperature of individual ZnO NRs/NWs synthesized at 80 °C and treated CTA or AUT to 100 ppm of hydrogen gas. Response in dynamic mode at 150 °C to 100 ppm of H_2 gas of a single ZnO NRs/NWs synthesized at 80 °C and treated by: (b) CTA or (c) AUT. (d) Gas response of the fabricated devices at 150 °C to 100 ppm of various gases and vapors (ammonia, *n*-butanol, 2-propanol, acetone, ethanol and hydrogen).

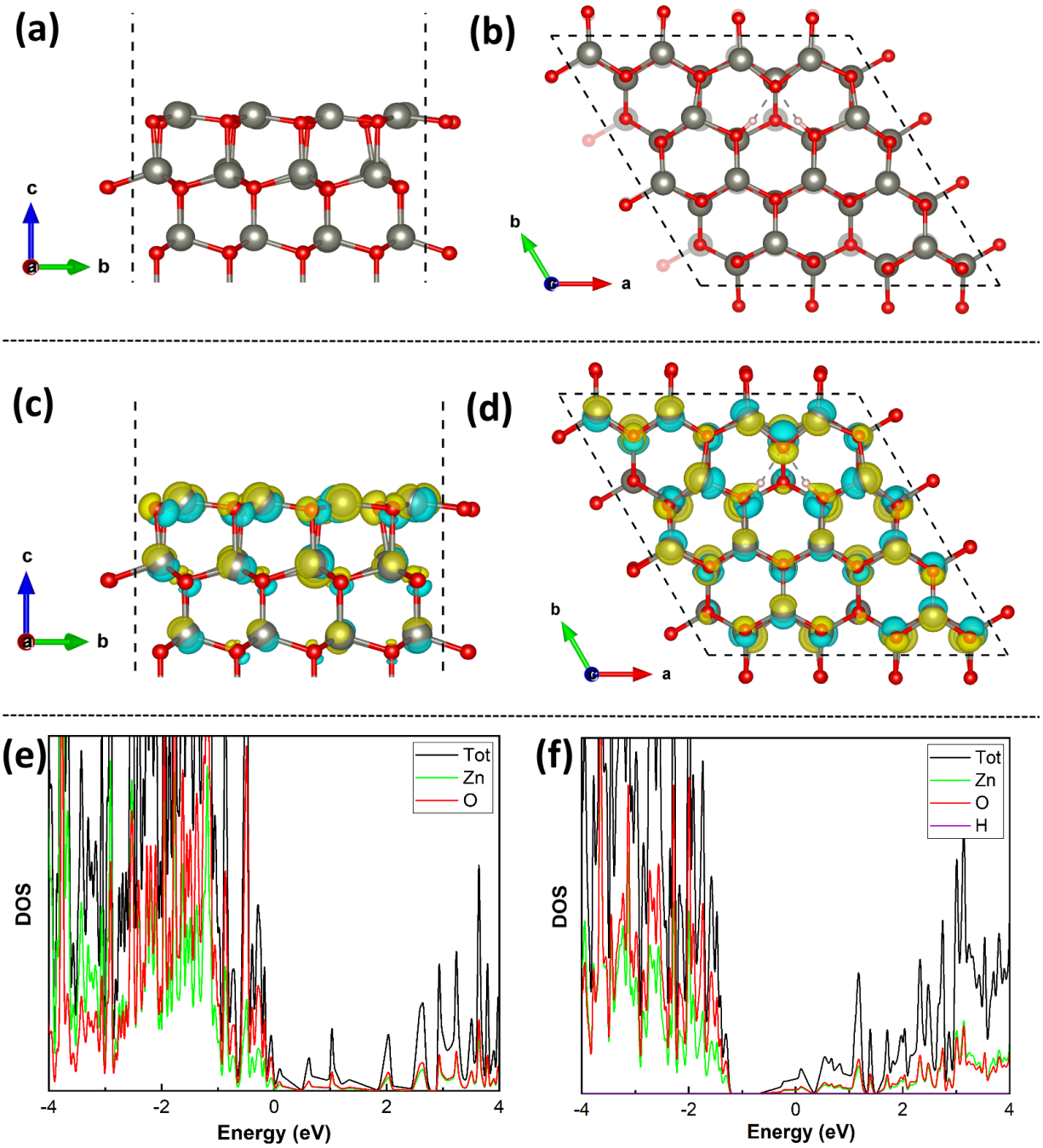

Figure 11. Interaction of hydrogen gas molecule on ZnO (0001) surface with side (a) and top (b) views. Charge density difference plot of H_2 molecule interaction on ZnO (0001) surface with side (c) and top (d) views, where yellow and blue colors indicate positive and negative charge densities in (e/Bohr^3). Density of states for (e) ZnO (0001) surface and (f) of H_2 molecule over ZnO(0001) surface.

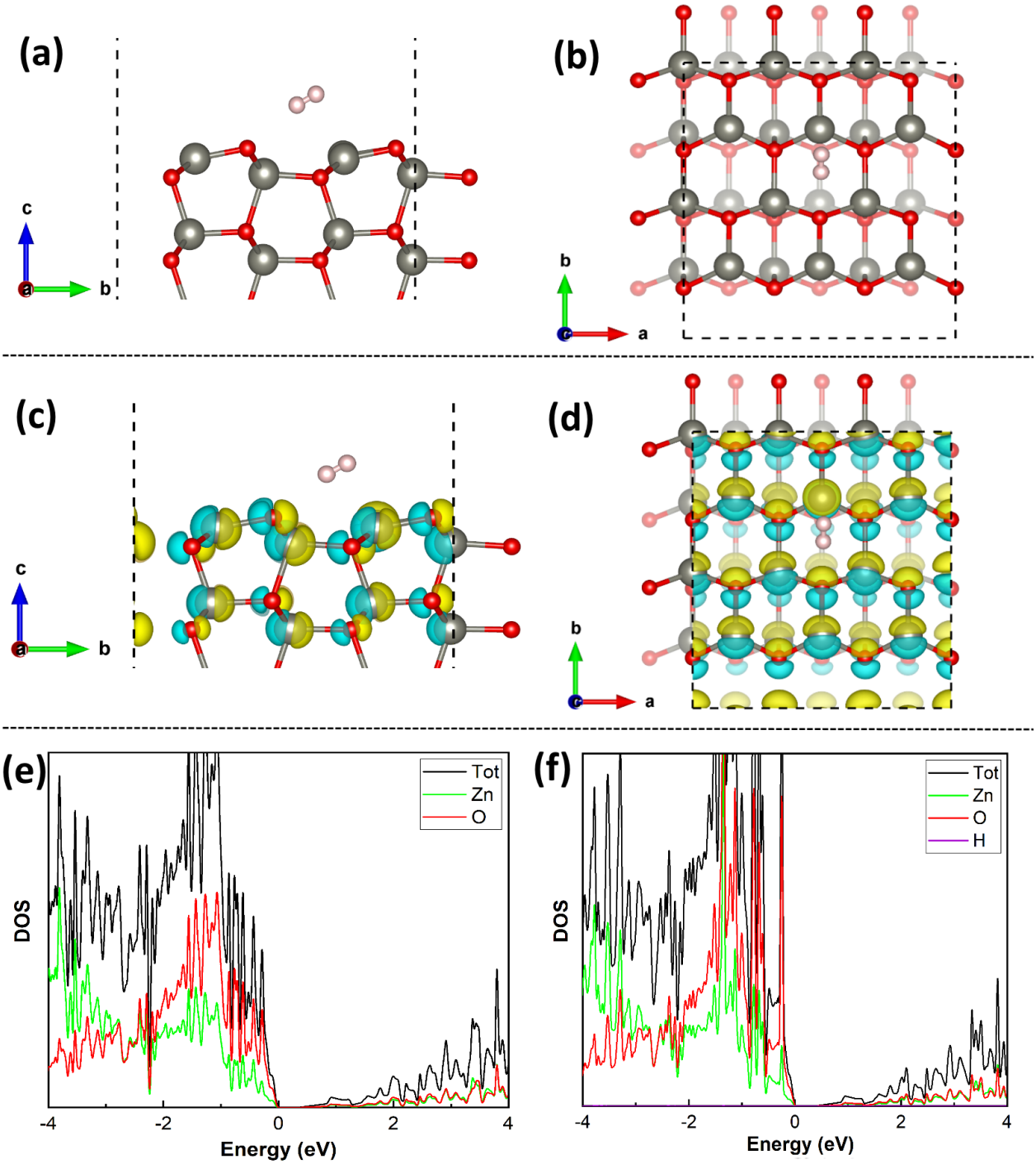

Figure 12. Interaction of H_2 molecule with ZnO $(10\bar{1}0)$ surface with side (a) and top (b) views. Charge density difference plot of hydrogen molecule interaction on ZnO $(10\bar{1}0)$ surface with side (c) and top (d) views, where positive and negative charge densities in (e/Bohr^3) are indicated by yellow and blue colors. Density of states of ZnO$(10\bar{1}0)$ surface (e) and of hydrogen molecule closed ZnO $(10\bar{1}0)$ surface (f).

Table 1. Relative concentration of ZnO, CO_2 and CO species calculated from the spectral area of the O-1s XPS binding energy region. The data correspond to samples annealed at different temperatures.

	ZnO (at %) (530.21 eV)	ZnO_x / $ZnO_x(OH)_y$ (at %) (531.61 eV)	CO (at %) (531.11 eV)	CO_2 (at %) (532.51 eV))
(i) OLU105_As-grown	42.8	27.3	22.3	7.6
(ii) OLU105_AUT	53.8	10.2	23.6	12.4
(iii) OLU103_As-grown	53.1	32.9	9.9	4.1
(iv) OLU103_AUT	49.2	28.6	15.9	6.3